A glycine zipper motif governs translocation of type VI secretion toxic effectors across the cytoplasmic membrane of target cells

Jemal Ali[1,2,3], Manda Yu[1#], Li-Kang Sung[1], Yee-Wai Cheung[1], and Erh-Min Lai[1,2,4*]

[1] Institute of Plant and Microbial Biology, Academia Sinica, Taipei, Taiwan
[2] Molecular and Biological Agricultural Sciences Program, Taiwan International Graduate Program, National Chung-Hsing University and Academia Sinica, Taipei, Taiwan
[3] Graduate Institute of Biotechnology, National Chung-Hsing University, Taichung, Taiwan
[4] Biotechnology Center, National Chung-Hsing University, Taichung, Taiwan

Running title: Glycine zipper mediated effector entry

* Corresponding author
Institute of Plant and Microbial Biology, Academia Sinica
128, Sec. 2, Academia Road, Nankang, Taipei, Taiwan 115201
Tel: 886-2-27871158
E-mail: emlai@gate.sinica.edu.tw

#Current address
Department of Biological Sciences
University of Wisconsin-Milwaukee
Milwaukee, Wisconsin, USA

ABSTRACT

Type VI secretion systems (T6SSs) can deliver diverse toxic effectors into eukaryotic and bacterial cells. Although much is known about the regulation and assembly of T6SS, the translocation mechanism of effectors into the periplasm and/or cytoplasm of target cells remains elusive. Here we use the *Agrobacterium tumefaciens* DNase effector Tde1 to unravel the mechanism of translocation from attacker to prey. We demonstrate that Tde1 binds to its adaptor Tap1 through the N-terminus, which harbours continuous copies of GxxxG motifs resembling the glycine zipper structure found in proteins involved in the membrane channel formation. Amino acid substitutions on $G^{39}xxxG^{43}$ motif does not affect Tde1-Tap1 interaction and secretion but abolish its membrane permeability and translocation of its fluorescent fusion protein into prey cells. The data suggest that $G^{39}xxxG^{43}$ governs the delivery of Tde1 into target cells by permeabilizing the cytoplasmic membrane. Considering the widespread presence of GxxxG motifs in bacterial effectors and pore-forming toxins, we propose that glycine zipper mediated permeabilization is a conserved mechanism used by bacterial effectors for translocation across target cell membranes.

Key words: Type VI secretion system, DNase effector, antibacterial, glycine zipper, translocation, *Agrobacterium tumefaciens*

INTRODUCTION

In a complex microbial community, bacteria have evolved versatile secretion systems for export or import of substrates across their membranes in response to different environmental cues. Each specialized protein secretion systems (type I to X secretion system [TISS to TXSS])(reviewed in Christie, 2019; Costa et al., 2015; Palmer et al., 2020) can recognize specific substrates for secretion and translocation across one or multiple membranes. The type VI secretion system (T6SS) is a molecular weapon deployed by many Proteobacteria for pathogenesis, antagonism, or nutrient acquisition (Coulthurst,

57 2019). The T6SS effectors discovered so far exert functions in antibacterial, anti-
58 eukaryotic, and metal acquisition (Hachani et al., 2016; Jurenas and Journet, 2021; Lien and Lai,
59 2017; Russell et al., 2014). The most established T6SS effectors are bacterial toxins, in which
60 bacteria also produce cognate immunity proteins to prevent self-intoxication and toxicity
61 in the sibling cells.

62 T6SS is a multiprotein complex, composed of at least 13 conserved core proteins
63 resembling a phage tail structure, that extends from the cytoplasm to the outer membrane
64 of the attacker cell (Cherrak et al., 2019; Wang et al., 2019). The T6SS machine consists of the
65 Tss(J)LM membrane complex (MC), TssEFGK base plate (BP), TssBC contractile sheath,
66 and Hcp-VgrG-PAAR puncturing device. The MC interacts with the BP (Cherrak et al., 2018;
67 Durand et al., 2015), which serves as a docking site of VgrG-PAAR effector complex to
68 initiate polymerization of the tail (Zoued et al., 2016). The tail is composed of the Hcp inner
69 tube and TssBC outer sheath, whose biogenesis is regulated by TssA cap protein, and
70 when triggered, the sheath contracts and ejects out the effector decorated puncturing
71 device into extracellular milieu or target cells (Ali and Lai, 2022; Basler et al., 2012; Vettiger and
72 Basler, 2016).

73 The T6SS has multiple strategies for delivering diverse effectors. On the basis of the
74 known effectors and their transport mechanisms, effectors can be classified as
75 "specialized" or "cargo" effectors (Cherrak *et al.*, 2019; Cianfanelli et al., 2016). Specialized
76 effectors are fused to either of the C-termini of three core structural proteins (Hcp, VgrG,
77 or PAAR) while cargo effectors interact directly or require a specific chaperone/adaptor
78 to be loaded into the lumen of the Hcp tube or onto the VgrG spike prior to secretion.
79 Though diverse T6SS antibacterial effectors that act in the cytoplasm, membrane, or
80 periplasm of the target cells have been reported (Jurenas and Journet, 2021; Lien and Lai, 2017;
81 Russell *et al.*, 2014), their mechanisms to breach outer and inner membranes for targeting
82 cytoplasm of their targets still yet to be clarified.

83 A glycine zipper structure consisting of repetitive GxxxG motifs is commonly found in
84 membrane-associated proteins (Kim et al., 2005) and bacterial toxins (Fonte et al., 2011; Kim
85 et al., 2004). Glycine zipper motifs are known be involved in toxicity of some bacterial
86 effectors for membrane channel formation. For example, the transmembrane domain

87 (TMD) of a vacuolating toxin, VacA of *Helicobacter pylori* encodes three GxxxG motifs
88 forming helix-helix packing interactions (Kim *et al.*, 2004), which are required for the
89 vacuolation and membrane channelling contributing to VacA toxicity (McClain et al., 2003).
90 Type I secretion effectors CdzC and CdzD of *Caulobacter crescentus* and T6SS effector
91 Tse4 of *Pseudomonas aeruginosa,* also possess glycine zipper motifs involved in
92 antibacterial activity (Garcia-Bayona et al., 2017; LaCourse et al., 2018). Expression of Tse4
93 disrupted the proton motive force of the inner membrane while CdzC and CdzD form
94 surface aggregation for contact-dependent killing of target cells. However, how glycine
95 zipper motifs of Tse4 and CdzCD involved in toxicity remain unknown.

96 A T6SS-encoding locus is highly conserved in the genome of plant pathogenic bacterium
97 *Agrobacterium tumefaciens* and the apparatus functions as an antibacterial weapon (Chou
98 et al., 2022; Ma et al., 2014; Wu et al., 2021; Yu et al., 2020). We previously revealed that *A.*
99 *tumefaciens* strain C58 deploys two Type VI DNase effectors (Tde1 and Tde2) as the
100 major antibacterial weapons, in which the cognate immunity proteins (namely Tdi1 and
101 Tdi2) prevent autointoxication (Ma *et al.*, 2014). Both Tde1 and Tde2 harbour a novel C-
102 terminal Ntox15 toxin domain (Zhang et al., 2012) containing an HxxD catalytic motif required
103 for its DNase activity (Ma *et al.*, 2014). Tde1 requires its cognate chaperone/adaptor Tap1
104 for loading onto VgrG1 for secretion (Bondage et al., 2016).

105 By obtaining the uncoupling Tde1 variants that remain capable for binding to Tap1 for
106 export but deficient in membrane permeability, translocation, and interbacterial
107 competition, we reveal the secretion and translocation mechanism of Tde1 from the
108 attacker cell to the target cell. We show that the N-terminal region of Tde1 harbouring
109 repetitive glycine zipper motifs is sufficient for interacting with Tap1 for secretion. Once
110 secreted, a conserved glycine zipper motif is necessary for translocation across target
111 cell membranes. The findings demonstrate a new role of glycine zipper motif(s) in effector
112 delivery into target cells.

113

114 **RESULTS**

115 **Tde1 can cause DNase-independent growth inhibition in *Escherichia coli***

116 Our previous study showed that overexpression of Tde1 in *A. tumefaciens* C58 caused
117 growth inhibition, and the immunity protein Tdi1 only partially protected against this
118 cytotoxicity (Ma *et al.*, 2014). We hypothesized that Tde1 has domains apart from the DNase
119 domain that contribute to its toxicity. In addition to the C-terminal Ntox15 DNase domain
120 (amino acid 99-247) (Ma *et al.*, 2014), Tde1 has a predicted transmembrane domain (TMD,
121 22-42) (Fig.1A). Thus, three fragments of Tde1, that being the N-terminal, N-Tde1(1-97)
122 and two C-terminal regions, C1-Tde1(49-278), and C2-Tde1(98-278) were tested for
123 toxicity. To avoid confounding effects by the DNase activity, substitutions of catalytic
124 residues (H190A, D193A) were introduced in the C1-Tde1 and the full length wide-type
125 Tde1 to become C1-Tde1(M) and Tde1(M) respectively (Fig.1A). Ectopic expression in *E.*
126 *coli* (DH10B) under an IPTG inducible promoter showed that N-Tde1 was sufficient to
127 inhibit growth (Fig.1B). Tde1(M), but not the C1-Tde1(M), is growth inhibitory. Although
128 C2-Tde1(WT) retains the wild type DNase catalytic residues, it was not able to inhibit
129 growth, suggesting the N-terminus is required for the DNase activity. Both C1-Tde1(M)
130 and C2-Tde1(WT) are expressed at levels similar or higher than N-Tde1 or Tde1(M),
131 indicating that their loss of growth inhibition is not due to non-expression of the proteins
132 (Fig. S1A). Evidence suggests the N-terminal region of Tde1 is sufficient to confer toxicity
133 under conditions tested and that the C-terminal DNase domain requires entire or part of
134 the N-terminus for it to cause toxicity.

135 To test whether Tdi1, the immunity protein for the DNase toxicity of Tde1 (Ma *et al.*, 2014),
136 can also neutralize the N-Tde1 toxicity, the Tde1 variants were co-expressed with the
137 Tdi1. The result show that Tdi1 could not rescue the growth inhibition caused by the N-
138 Tde1 and Tde1(M) (Fig. 1C, Fig. S1B). This indicates that Tdi1 cannot neutralize the N-
139 terminus-mediated toxicity.

140 **A glycine zipper motif in N-terminus of Tde1 is required for toxicity and enhanced**
141 **membrane permeability**

142 To get an insight into the cause of growth inhibition by N-terminus of Tde1, we used N-
143 Tde1 region as a query to search against the NCBI non redundant (nr) database and
144 identified Tde1 homologues encoded in the T6SS gene clusters of
145 *Agrobacterium/Rhizobium* as well as tape measure proteins (TMP) encoded in genomes

146 of *Paraburkholderia/Burkholderia* (Fig. 1D, Fig, S2). We noticed the conservation of
147 continuous copies of GxxxG motifs (12-51) in the N-terminus of Tde1, which resembles
148 the glycine zipper motifs overrepresented in membrane proteins and reported to be
149 involved in the membrane channel formation (Kim *et al.*, 2005). Thus, we hypothesized that
150 these repetitive glycine zipper motifs are involved in membrane permeability and N-Tde1
151 toxicity.

152 To verify the hypothesis, two highly conserved glycine residues at position 39 and 43 of
153 a glycine zipper motif were substituted with leucine (G39L and G43L), and the resulting
154 N-Tde1 and Tde1(M) variants were named as N-Tde1^{GLGL}, Tde1(M)^{GLGL} respectively. The
155 growth analysis of *E. coli* DH10B cells by counting viable cells and OD_{600} measurement
156 showed that both N-Tde1^{GLGL} and Tde1(M)^{GLGL} lost the ability to cause growth inhibition
157 (Fig. 2A, Fig. S1C). Similar results were also observed when they were overexpressed in
158 *A. tumefaciens* Δ*tde1* mutant (Fig. S1D), indicating that the $G^{39}xxxG^{43}$ glycine zipper motif
159 of Tde1 is required for the observed toxicity.

160 Next, we tested whether N-Tde1 can increase *E. coli* inner membrane permeability. To
161 do so, we used the β-galactosidase activity assay to measure the entry of ortho
162 nitrophenyl galactopyranoside (ONPG) (301 Da) into the cytosol. ONPG normally
163 requires a functional permease LacY to enter into the cytosol but can enter if the inner
164 membrane is permeabilized/compromised (Casteels et al., 1993; Epand et al., 2009). N-Tde1
165 and Tde1(M) as well as their glycine zipper substitution variants were expressed in *E. coli*
166 BW25113Δ*lacY* (Baba et al., 2006) carrying β-galactosidase (pYTA-*lacZ*). The
167 BW25113Δ*lacY*(pYTA-*lacZ*) complemented with *lacY* was used as a positive control. The
168 *E. coli* cells were induced with IPTG to express Tde1 variants for one hr and collected for
169 ONPG uptake assay. This time point was chosen because there is no obvious difference
170 on the number of viable cells among the strains tested (Fig. 2A, S1E). The results showed
171 that cells expressing either N-Tde1 or Tde1(M) had similar β-galactosidase activity as
172 LacY expressing cells. In contrast, cells expressing N-Tde1^{GLGL} and Tde1(M)^{GLGL} only
173 exhibited background level activity as the negative controls (Fig. 2B). These results
174 indicate that the N-Tde1 and Tde1(M) are able to increase membrane permeability
175 depending on the $G^{39}xxxG^{43}$ motif. The data also suggest that the N-terminus-mediated

176 growth inhibition is caused by its ability to enhance inner membrane permeability through
177 glycine zipper motifs.

178 To further analyse the extent of enhanced membrane permeabilization, cells from the
179 same experiment were normalized to the same OD_{600} and stained with Hoechst and
180 propidium iodide (PI). Hoechst (616 Da) is a nucleic acid staining dye which is permeable
181 to live Gram-negative bacterial cells while PI (668.4 Da) can only enter through a
182 compromised inner membrane or dead cells. The PI/Hoechst staining showed strong PI
183 signals in cells expressing N-Tde1 and Tde1 (M) but no or weak signals were detected in
184 cells expressing N-Tde1^{GLGL}, Tde1(M)^{GLGL}, or vector control, indicating that N-Tde1 is
185 able to enhance membrane permeability to allow molecules with size 668.4 Da to pass
186 (Fig. 2C).

187 We next determined whether the N-terminus of Tde1 is bacteriostatic or bacteriolytic by
188 growth recovery assay (Mariano et al., 2019). *E. coli* cells were induced with IPTG to express
189 N-Tde1 or Tde1(M) and after one hr, washed with fresh media without IPTG for
190 continuous cultivation. We found that growth was recovered when cells were washed of
191 the IPTG inducer, in contrast to the growth inhibition of cells with continuous IPTG
192 induction (Fig. 2D). Collectively, the data suggest that the N-terminus of Tde1 is sufficient
193 to facilitate membrane permeability for bacteriostatic toxicity, and such activity requires
194 the conserved $G^{39}xxxG^{43}$ glycine zipper motif.

195 **The N-terminus of Tde1 is necessary and sufficient for Tap1 interaction**

196 Tap1 is the adaptor for loading Tde1 onto VgrG1 (Bondage *et al.*, 2016; Ma *et al.*, 2014).
197 However, the region that Tde1 and Tap1 interact remains undefined. Thus, we performed
198 co-immunoprecipitation (co-IP) assay to identify the specific region of Tde1 that can
199 interact with Tap1 in *A. tumefaciens*. The HA-tagged Tde1 variants were expressed in
200 Δ*tde1* and anti-HA agarose bead was used to co-precipitate the interacting proteins
201 followed by western blotting to detect Tde1 variants and Tap1. The results showed that
202 the N-Tde1 and Tde1(M) interact with Tap1 but not the C-terminal variants, C1-Tde1(M)
203 and C2-Tde1 (Fig. 3A, Fig. S3). N-Tde1^{GLGL} and Tde1(M)^{GLGL} remain capable of
204 interacting with Tap1 (Fig.3A). The results suggest that Tap1 interacts with Tde1 through

205 the N-terminus and that the G39L and G43L substitution does not affect Tde1-Tap1
206 interaction.

207 **The N-terminus of Tde1 is necessary and sufficient for secretion**

208 Because N-Tde1 interacts with Tap1, we hypothesized that this region is required for Tde1
209 secretion. Thus, we performed secretion assay by expressing the various HA-tagged
210 Tde1 variants in Δ*tdei,* a deletion mutant lacking both *tde1-tdi1* and *tde2-tdi2* toxin
211 immunity pairs. Both cellular and extracellular fractions were collected to determine their
212 expression and secretion, respectively. The results showed that all Tde1 variants
213 containing N-terminus are secreted but not the C-terminus, C1-Tde1(M). The secretion is
214 in a T6SS-dependent manner as secretion was essentially abrogated in Δ*tdei*Δ*tssK,*
215 which lacks both *tdei* and *tssk* encoding the baseplate component. N-Tde1^{GLGL} and
216 Tde1(M)^{GLGL} are also stably expressed and secreted (Fig. 3B, Fig. S3). The data suggest
217 that N-terminus of Tde1 is necessary and sufficient for secretion and that the G39L and
218 G43L substitution does not interfere with the secretion capacity of Tde1. Accordingly,
219 Hcp secretion levels are highly correlated with Tap1-Tde1 interaction and secretion of
220 Tde1 variants (Fig. 3B). The data also confirmed the requirement of the Tap1-Tde1
221 interaction for Tde1 secretion and supported our previous finding that Tde loading onto
222 VgrG is critical for active T6SS secretion (Wu et al., 2020).

223 **G^{39}xxxG^{43} motif of Tde1 is required for target cell delivery**

224 Because the G^{39}xxxG^{43} glycine zipper motif located in N-Tde1 increased the membrane
225 permeability but was not required for secretion, we hypothesized that G^{39}xxxG^{43} is
226 responsible for inserting Tde1 into the inner membrane and delivering it into the
227 cytoplasm of target cells. Here, we engineered each of Tde1 variants fused to super-
228 folder green fluorescence protein (sfGFP) with a flexible (GGGS) linker between Tde1
229 and sfGFP to avoid the Tde1 functional/structural interference by GFP. The sfGFP fused
230 Tde1 variants were expressed in *A. tumefaciens* Δ*tdei* and Δ*tdei*Δ*tssK* mutants. The
231 secretion assay results showed that both WT and G39L and G43L substitution of N-Tde1-
232 sfGFP and Tde1(M)-sfGFP are secreted (Fig. S4A). No or trace amounts of proteins were
233 observed in the extracellular fractions of Δ*tdei1*Δ*tssk* mutants, demonstrating that the
234 secretion was T6SS dependent. C1-Tde1(M)-sfGFP protein signal could not be

235 unambiguously determined in the cellular fraction due to the overlapping of its predicted
236 protein band with cross-reacted proteins, and no corresponding C1-Tde1(M)-sfGFP band
237 was detected in the extracellular fraction. The secretion assay of Tde1 variants fused with
238 either HA or sfGFP concluded that N-Tde1 is necessary and sufficient for secretion and
239 the G39L and G43L substitution does not affect Tde1 being secreted, which is correlated
240 with the ability to interact with Tap1.

241 We next investigated the translocation of Tde1 variants by mixing *A. tumefaciens* Δ*tdei,*
242 expressing sfGFP-fused Tde1 variants, with *E. coli* cells expressing mCherry. *A.*
243 *tumefaciens* expressing sfGFP only (Vector-sfGFP) was used as a negative control. After
244 co-culture, we imaged populations for mCherry (false coloured in blue) and GFP (green)
245 to detect *E. coli* and *A. tumefaciens*, respectively. We merged images to identify cyan
246 colored cells (overlayed blue and green signals), which represent *E. coli* cells with
247 translocated Tde1 variants carrying sfGFP. We were able to observe ~50% of cells with
248 cyan fluorescence when *A. tumefaciens* expressing N-Tde1-sfGFP and Tde1(M)-sfGFP
249 was co-cultured with *E. coli* mCherry whereas the GFP and mCherry signals were not
250 overlapped in the *E. coli* cells co-cultured with *A. tumefaciens* strains expressing GFP
251 only or sfGFP-fused C1-Tde1(M), N-Tde1^{GLGL}, Tde1(M)^{GLGL} respectively (Fig. 4). No cyan
252 fluorescence was observed when N-Tde1-sfGFP and Tde1(M)-sfGFP were expressed in
253 the Δ*tdei1*Δ*tssk* mutant as the attacker (Fig. S4B).

254 The data suggest that Tde1 is translocated into target cells in a T6SS- and G^{39}xxxG^{43}-
255 dependent manner. Because N-Tde1^{GLGL}-sfGFP and Tde1(M)^{GLGL}-sfGFP could be
256 secreted but not translocated into target cells, G^{39}xxxG^{43} motif is necessary for delivering
257 Tde1 into the target cell.

258 **G^{39}xxxG^{43} is critical for interbacterial competition but not for DNase activity**

259 To assess the role of the G^{39}xxxG^{43} motif for target cell intoxication in the context of
260 interbacterial competition, *A. tumefaciens* C58 Δ*tdei* expressing either Tde1-Tdi1,
261 Tde1(M)-Tdi1, or single/double G39L and G43L substitution variants, was competed with
262 target *E. coli* (DH10B) cells. By counting the survival rate of *E. coli* prey cells, the data
263 showed that *A. tumefaciens* Δ*tdei* (Tde1-Tdei1*)* exhibits an antibacterial activity but not in
264 the negative controls, the secretion deficient mutants Δ*tssL* and Δ*tdei*Δ*tssK* (Tde1-Tdei1*)*

265 (Fig. 5A). No antibacterial activity could be observed for *A. tumefaciens* Δ*tdei* expressing
266 Tde1(M)-Tdi1, indicating the DNase-mediated killing to *E. coli*. The antibacterial activity
267 of Δ*tdei*(Tde1^{GLGL}-Tdi1, Tde1^{G39L}-Tdi1, Tde1^{G43L}-Tdi1*)* was not detectable, similar to that
268 of negative controls. We also performed interbacterial competition assays using *A.*
269 *tumefaciens* strain 1D1609, which is susceptible to T6SS killing by C58 (Wu et al., 2019).
270 The interbacterial competition between two *A. tumefaciens* strains was calculated by
271 competitive index, which revealed the higher competitiveness of Δ*tdei* (Tde1-Tdi1*)* and
272 C58 against 1D1609 but no competitive advantage could be detectable for any of glycine
273 zipper variants or Tde1(M) (Fig. 5B). The observed antibacterial activity is T6SS-
274 dependent because the killing activity of Tde1 was not observed when expressed in
275 Δ*tdei*Δ*tssK.* The results indicate that $G^{39}xxxG^{43}$ motif is required for interbacterial
276 competition at both inter- or intra-species levels. We also performed a secretion assay of
277 these *A. tumefaciens* attacker strains and all glycine zipper variants were secreted (Fig.
278 5C). It is notable that Tde1^{GLGL} proteins accumulated at slightly lower levels while
279 Tde1^{G39L} and Tde1^{G43L} had similar or even higher protein levels to that of Tde1 and
280 Tde1(M). Accordingly, Tde1^{GLGL} was secreted at lower levels.

281 To exclude the possibility that G39L and G43L substitution may influence its DNase
282 activity, we performed *in vivo* plasmid DNA degradation assay. Tde1 and the variants
283 were each expressed by tightly controlled arabinose-inducible promoter for *in vivo*
284 plasmid DNA degradation assay in *E. coli* BW25113 as described (Ma *et al.*, 2014). It was
285 observed that plasmid DNA was completely degraded in cells expressing Tde1, but not
286 in the negative controls, the cells without arabinose induction nor cells expressing
287 Tde1(M). Plasmid DNA was also degraded by Tde1^{GLGL} but not as complete as Tde1
288 while both Tde1^{G39L} and Tde1^{G43L} exhibit wild-type level DNase activity. (Fig. 5D). The
289 lower DNA degradation efficiency of Tde1^{GLGL} could be correlated with the barely
290 detected Tde1^{GLGL} proteins (Fig. 5D). We also found that the degree of plasmd DNA
291 degration is also correlated with the growth inhibition effect (Fig. 5E and Fig. S1E). The
292 slightly recovery of Tde1^{GLGL} from growth inhibition is consistent with the instability of
293 Tde1^{GLGL}. The evidence that G39L and G43L substitutions abolished interbacterial
294 competition but did not affect DNase activity and secretion of Tde1 suggest the $G^{39}xxxG^{43}$

295 motif is necessary for delivering Tde1 across the inner membrane into the cytoplasm of
296 target cells.

297

298 **DISCUSSION**

299 Through the dissection of Tde1 DNase effector, we provide strong evidence for a role of
300 the N-terminal glycine-zipper motif(s) of Tde1 in delivering the T6SS effector into target
301 cells. Here, we propose a model explaining the loading, firing, and translocation of Tde1
302 (Fig.6). In *A. tumefaciens,* Tde1 DNase activity is neutralized by Tdi1 by binding to C-
303 terminal DNase domain while its N-terminal domain interacts with Tap1 for loading onto
304 VgrG1 (Step 1). The VgrG1-Tap1-Tde1-Tdi1 complex is then recruited onto membrane-
305 associated baseplate, which serves as a docking site for polymerization of Hcp tube and
306 TssBC sheath (Step 2). Upon TssBC sheath contraction (Step 3), Tap1 and Tdi1 may fall
307 off and Hcp-VgrG-Tde1 puncturing device is then ejected for secretion. In contact with a
308 target cell, Tde1 may be delivered to periplasm of the target cell where Tde1
309 permeabilises the inner membrane in a $G^{39}xxxG^{43}$ motif-dependent manner (Step 5).
310 Once delivered, Tde1 exerts its toxicity by attacking DNA for degradation (Step 6).

311 T6SS cargo effectors often require the specific chaperone/adaptor for loading onto
312 puncturing device for secretion. Our previous findings demonstrated that Tap1, a
313 DUF4123-containing protein, specifically interacts with Tde1 for loading onto VgrG1 for
314 secretion (Bondage *et al.*, 2016; Ma *et al.*, 2014). We now show that N-terminal region of Tde1
315 is necessary and sufficient for interaction with Tap1 for secretion and delivery into target
316 cells. The evidence that $Tde1^{GLGL}$ variant remains capable for binding to Tap1 for export
317 but deficient in membrane permeability and translocation demonstrate a distinct role of
318 this $G^{39}xxxG^{43}$ motif in target cell delivery. Among the nine classes of the Ntox15-
319 containing proteins, the majority of them including Tde1 belong to class I without
320 detectable N-terminal domains (Fig. S2). We identified the presence of glycine zipper
321 motifs overlapping with transmembrane domain (TMD) not only in N-terminal region of all
322 Tde1 orthologs encoded in Rhizobiaceae but also in C-terminal region of tape measure
323 proteins (TMP) encoded in genomes of *Paraburkholderia/Burkholderia,* likely as a
324 prophage. TMP is a phage protein suggested to have a channel forming activity (Roessner

325 and Ihler, 1984; 1986) and as a determinant in connecting host inner membrane proteins for
326 injecting phage genome into bacterial host cells (Cumby et al., 2015). Such conservation in
327 Tde1 orthologs suggests that this glycine zipper-mediated delivery could be a common
328 strategy deployed by these bacterial effectors for translocation across target cell
329 membranes. It would be also interesting to investigate whether TMP also employs its C-
330 terminal glycine zipper to mediate phage genome entry into host cells.

331 A role of N-terminal domain involved in translocation of polymorphic toxins have been
332 well documented in those of contact-dependent growth inhibition (CDI) system and
333 bacteriocins (Ruhe et al., 2020). However, little is known for the translocation mode of
334 bacterial toxins delivered by other systems. Previous study in *P. aeruginosa* showed that
335 VgrG-loaded Tse6-EgaT6 complex is sufficient to translocate across a lipid bilayer *in vitro*
336 (Quentin et al., 2018), suggesting a role of VgrG-effector complex itself in inserting across
337 the inner membrane of target cells. A recent study further uncovered a widespread
338 prePAAR motif in N-terminal TMDs of T6SS effectors involved in interaction with Eag
339 family chaperone for export (Ahmad et al., 2020). The findings from the Tap1 and Eag
340 chaperone-mediated T6SS toxins led us to propose that the bacterial toxins harbouring a
341 N-terminal TMD may be protected by its cognate chaperone/adaptor from insertion into
342 membranes in the attacker cell. However, once the effector is injected into the periplasm
343 of the target cell, specific motifs (such as glycine zippers or perhaps prePAAR) may insert
344 into the inner membrane for the delivery into the cytoplasm. By an elegant *in vitro*
345 translocation assay, a recent study discovered a N-terminal domain of a bacteriocin
346 pyocin G is required for import of its C-terminal nuclease toxin into the cytoplasm cross
347 inner membrane (Atanaskovic et al., 2022). This inner membrane translocation domain (IMD)
348 is distinct from the glycine zipper repeats identified in this study but also found conserved
349 in other bacterial toxins including some of T6SS. Thus, bacterial toxins itself directing
350 translocation into target cells could be a general strategy used by bacteria for
351 interbacterial competition.

352 A few membrane permeabilizing T6SS toxins have been reported. The *Vibrio cholerae*
353 VasX caused dissipation of membrane potential, leading to membrane permeabilization
354 of target bacterial cells similar to the Tme effectors of *V. parahaemolyticus,* which

355 represents a widespread family of T6SS effectors harbouring C-terminal TMD for
356 membrane disruption (Fridman et al., 2020; Miyata et al., 2013). On the other hand, Tse4
357 disrupts the membrane potential and forms a cation selective pore without membrane
358 permeabilization where the pore cannot even allow the permeability of a relatively smaller
359 molecular weight (ONPG, 300 Da) (LaCourse *et al.*, 2018). Distinct from these toxins in which
360 they confer pore forming activity for toxicity, the role of glycine zipper(s) of Tde1 appears
361 to enhance membrane permeability for bringing the toxin domain into target cell
362 cytoplasm because Tde1(M) with complete glycine zipper motifs but loss of DNase
363 activity did not show interbacterial competition activity against *E. coli* or *A. tumefaciens*
364 under conditions tested (Fig. 5A, 5B) (Ma *et al.*, 2014).

365 To date, no structural information is available for Ntox15 superfamily proteins where Tde1
366 belongs. While N-terminus of Tde1 lacks sequence similarity to any of those known pore-
367 forming toxins, structural modelling showed structural similarity of two helixes containing
368 consecutive glycine zipper motifs to the pore forming domain of pyocin S5 (Behrens et al.,
369 2020) (Fig.S6). Pyocin S5 can cause ATP leakage and PI permeability (Ling et al., 2010)
370 potentially to inner membrane after translocation through FptA and TonB1 (Behrens *et al.*,
371 2020). Tde1 allows the passage of relatively larger molecule, PI (668 Da), suggesting that
372 its N-terminal glycine zipper(s) may form larger pores similar to pyocin S5. $G^{39}xxxG^{43}$
373 motif plays no role in DNase activity of Tde1 but is crucial for its protein stability. Tde1
374 with substitution of one of the two glycine residues to leucine retains stability of intact
375 proteins but Tde1 is prone for truncations and degradation when both glycine residues
376 are substituted to leucine. The instability is most evident when ectopically expressed in
377 *E. coli* and when retaining DNase activity (Fig. S1A, Fig. 5). Single glycine substitution
378 ($Tde1^{G39L}$ and $Tde1^{G43L}$ variants) does not influence protein stability may suggest that the
379 adjacent glycine residues (G^{35} or G^{47}) are sufficient to compensate the loss of one glycine
380 of $G^{39}xxxG^{43}$ motif for structural integrity in both variants. The importance of $G^{39}xxxG^{43}$
381 motif in Tde1 protein stability is consistent with the role of glycine zippers in structural
382 impact (Kim *et al.*, 2005). However, integrity of $G^{39}xxxG^{43}$ motif is critical for interbacterial
383 competition because both $Tde1^{G39L}$ and $Tde1^{G43L}$ variants do not exhibit detectable
384 antibacterial activity to either *E. coli or A. tumefaciens* (Fig. 5A, 5B). These results suggest

385 the role of $G^{39}xxxG^{43}$ motif in delivering Tde1 across the inner membrane into the
386 cytoplasm of target cells.

387 It is striking to observe such a high percentage of cells (~50%) representing N-Tde1-
388 sfGFP and Tde1(M)-sfGFP translocation from *A. tumefaciens* into *E. coli* cells expressing
389 mCherry (Fig. 4). Adding the flexible GGGS linker between sfGFP and Tde1 that retain
390 both Tde1 secretion activity and GFP fluorescence may be the key for the success of this
391 translocation experiment. Interestingly, we also observed many GFP foci from *A.*
392 *tumefaciens* cells expressing translocation competent N-Tde1-sfGFP or Tde1(M)-sfGFP
393 while others including *E. coli* cells with GFP signals uniformly distributed throughout the
394 cells. Based on the role of glycine zippers in interacting with membrane, we propose that
395 Tde1 proteins may preferentially bind to microdomain of cytoplasmic membrane, which
396 was recently found in *A. tumefaciens* (Czolkoss et al., 2021). We also found that Tde1
397 proteins (either tagged with HA or GFP, Fig. 3, S1, S4A) are prone for truncation
398 especially when they are ectopically expressed in *E. coli* or when Tdi1 is absent or not
399 equivalent. Thus, it is possible that Tde1-GFP proteins are truncated after translocation
400 into *E. coli* cells, in which most GFP signals are emitted from free GFP instead of Tde1-
401 GFP. The stability of free GFP derived from translocated Tde1-GFP may also explain the
402 high percentage of *E. coli* cells exhibiting overlayed GFP/mCherry signals. There is
403 evidence that truncation of T6SS effectors is critical for the toxicity (Pei et al., 2020). Future
404 work to investigate how Tde1 interacts with membrane and dissect the region required
405 for DNase activity shall shed light to understand the biological significance and
406 mechanisms underlying this interesting observation.

407 With the knowledge of effector translocation mechanisms, the bacterial protein secretion
408 apparatus also offers a strategy for delivering heterologous proteins to specific cells.
409 T6SS is a promising vehicle for such purpose because effectors or secreted proteins
410 appear to be delivered with their folded or partially folded form, unlike those to be
411 transported as unfolded forms in most of other specialized secretion systems (Costa *et al.*,
412 2015). Engineering T6SS carriers such as VgrG spikes to carry exogenous effectors
413 proteins into target cells are feasible but challenging (Ho et al., 2017; Wettstadt and Filloux,
414 2020; Wettstadt et al., 2020). By using a truncated variant of PAAR, a recent study showed

415 delivering exogenous T6SS effectors and Cre recombinase for genetic modification in the
416 target cells (Hersch et al., 2021). Our success in using N-Tde1 in the delivery of sfGFP
417 proteins into target *E. coli* cells where they exert fluorescence also suggest potential
418 applications of N-Tde1 for the delivery of proteins of interests such as genetic modifiers.
419 This strategy provides advantages over transforming foreign DNA for expressing a protein
420 of interest from creating undesired genome manipulation.

421

422 **MATERIALS AND METHODS**

423 **Strains and growth conditions**

424 The strains and plasmids used in this study are listed in the supplementary Tables S1and
425 S2. The *E. coli* strains used in this study are BW25113 and DH10B. All the *A. tumefaciens*
426 strains were cultured on 523 medium (Kado, 1970) at 28 °C unless stated. The *E. coli* strains
427 were cultured on Luria Bertani (LB) medium (10 g L−1 NaCl, 10 g L−1 tryptone, and 5 g
428 L−1 yeast extract) at 37°C unless stated. Where appropriate, the media were
429 supplemented with 100 µg mL^{-1} spectinomycin, gentamycin 25 µg mL^{-1} (for *E. coli*) and
430 50 µg mL^{-1} (for *A. tumefaciens*), 50 µg mL^{-1} ampicillin, 50 µg mL^{-1} kanamycin, 1 mM
431 Isopropyl β- d-1-thiogalactopyranoside (IPTG).

432 **Growth inhibition assay**

433 For growth inhibition assay of IPTG-inducible expression of Tde1 and its variants, *E. coli*
434 (DH10B) harbouring pTrc200 vector or the derivatives expressing Tde1 variants were
435 grown overnight in LB medium supplemented with spectinomycin prior to 1:30 dilution in
436 a fresh medium and incubated for 2 hrs at 37°C with 250 rpm. After 2 hrs, the cultures
437 were normalized to OD_{600} 0.1 in LB with 1 mM IPTG for continuous culture in the same
438 growth condition. The growth of *E. coli* was monitored for OD_{600} every one hr using
439 ULTROSPEC® 10 cell density meter (Biochrom, UK) or viable cell by counting colony
440 forming units (CFUs) on LB agar containing Sp. For growth inhibition assay of arabinose-
441 inducible expression, *E. coli* BW25113 harbouring pJN105 vector or the derivatives
442 expressing Tde1 variants were used. Overnight cultures of *E. coli* cells were adjusted to
443 an OD_{600} of 0.1 in 200 µL LB with 0.2% L-arabinose in a 96-well plate. The OD_{600} values

444 were measured by the Synergy H1 microplate reader (Agilent Technologies, USA) with
445 agitation at 37 °C. The OD_{600} values or CFUs of indicated time points were used to
446 calculate mean ± SD of three independent repeats. One way Analysis of Variance
447 (ANOVA) was used for the analysis of statistical significance followed by the Tukey's
448 multiple comparison.

449 ***In vivo* plasmid DNA degradation assay.** The *in vivo* plasmid DNA degradation assay
450 was performed as described (Ma *et al.*, 2014) with minor modifications. Briefly, overnight
451 cultures of *E. coli* BW25113 carrying pJN105 vector or the derivatives expressing Tde1
452 variants were adjusted to an OD_{600} of 0.3 in 4 mL LB with 0.5% D-glucose or 0.2% L-
453 arabinose. After induction for 3 hrs, bacterial cells normalized by OD_{600} were collected for
454 plasmid DNA extraction and western blot analysis. The plasmids were then extracted and
455 applied to 0.6% agarose gel electrophoresis to detect the DNA degradation. The OD_{600}
456 values were measured by DEN-600 photometer (Biosan, Latvia) every hr.

457 **β-galactosidase and viability assays for ONPG update**

458 β-galactosidase assay was performed as described (Saint Jean et al., 2018) with minor
459 modifications. BW25113 wild type, BW25113Δ*lacY*(pYTA-lacZ), or BW25113Δ*lacY*
460 harbouring pTrc200 vector or the derivatives expressing Tde1 variants were grown
461 overnight and refreshed to a fresh medium as stated for growth inhibition assay. After
462 subculture for 2 hr, the cells were induced with 1 mM IPTG, and incubated for one more
463 hr. Part of the culture was adjusted to OD_{600} = 0.3 in Z-buffer and the Intracellular β-
464 galactosidase activity was measured by mixing 100 µL of 4 mg/ml ONPG with 900 µL of
465 the cells and incubation at room temperature for 10 min prior to measurement at OD_{420}.
466 The remaining cells were normalized to OD_{600} 0.3 in 0.9 % sterile saline and after serial
467 dilution, 10 µL was spotted on LB plate without antibiotics to recover the viable cells. Data
468 of OD_{420} were used to calculate mean ± SD of three independent experiments. One way
469 ANOVA was used for the analysis of statistical significance followed by the Tukey's
470 multiple comparison.

471 **Co-immunoprecipitation (Co-IP)**

472 The co-IP was performed according to the manufacturer's recommendations of EZview
473 red Anti-HA agarose (Sigma-E6779) with minor modifications. To identify Tap1 interacting
474 domain of Tde1, the HA tagged Tde1 variants were expressed on pTrc200 plasmid. For
475 co-IP in *A. tumefaciens,* C58 Δ*tde1* cells expressing the Tde1 variants grown in 523
476 medium overnight were resuspended in a 1:30 ratio to a fresh medium and incubated at
477 25°C for 3 hrs followed by 1 mM IPTG induction for additional 3 hrs. After 6 hrs post
478 incubation, the cells were normalized to OD_{600} of 5 per mL in ice-cold PBS buffer (pH 7.4).
479 After cell lysis by lysozyme treatment and sonication, the lysate was centrifuged and a
480 100 µL aliquot of the lysate was saved for the input fraction. The remaining 900 µL lysate
481 was mixed with 25 µL of pre-equilibrated Ezview red Anti-HA agarose and incubated at 4
482 °C for 1 hr. The beads were then washed 3 times with ice-cold PBS buffer and the proteins
483 bound to the beads were eluted with 100 µL of 2X SDS sample loading buffer. Similarly,
484 the aliquoted input fraction was mixed with equal volume of 2X SDS sample loading buffer
485 for analysis by western blotting.

486 **Secretion assay**

487 Type VI secretion assay was performed in 523 as described previously (Wu *et al.*, 2020).
488 Briefly, *A. tumefaciens* strain was cultured overnight in 523 medium and normalized to
489 OD_{600} of 0.2 in a fresh medium. After 6 hrs of culturing, the secreted proteins were
490 collected by centrifuging at 10,000 g for 5 mins. The resulting pellet was adjusted to OD_{600}
491 of 10 as a cellular fraction. The culture supernatant was filtered with 0.22 µm Millipore
492 filter membrane and resulting filtrate was subjected for TCA precipitation (Wu et al., 2008)
493 and referred as an extracellular fraction.

494 **Western blotting**

495 Western blot analyses were done as previously described (Lin et al., 2013). The following
496 primary antibody titres used were: HA epitope (1:4,000), Tap1 (1:3,000) (Lin *et al.*, 2013),
497 Strep (1:4,000), EF-Tu (1:6,000), and C-terminal Tde1 (1:4,000) (Bondage *et al.*, 2016; Ma *et*
498 *al.*, 2014), Hcp (1:2,500) (Wu *et al.*, 2008).

499 **Interbacterial competition assays**

500 For interbacterial competition with *E. coli* (target), *A. tumefaciens* strain (attacker) was
501 grown overnight at 28°C in 523 broth with appropriate antibiotics if needed. *E. coli* DH10B
502 harbouring pRL662 plasmid was grown at 37°C in LB broth with gentamycin. After
503 harvesting and washing the cells in 0.9% saline, the attacker to target cell density was
504 adjusted to 30:1 (OD_{600} =3: 0.1) and the mix was spotted on Agrobacterium kill-triggering
505 (AK) (Yu *et al.*, 2020) or LB medium containing 1.5% (wt/vol) agar. After incubation of the
506 mixed strains for 16 hr at 28°C, the spot was resuspended in 0.9% saline, serial diluted,
507 and spotted on a gentamycin-containing LB agar square plate at 37°C to calculate *E. coli*
508 survival rate by CFU counts. Similar procedure was used when using *A. tumefaciens*
509 strain 1D1609 as a target, which was grown at 28°C in 523 broth prior to competition. The
510 competition was carried out on AK medium for 16 hr at 28°C with CFU counting at both
511 initial and final time points by selection of C58 strains with Sp resistance and 1D1609 with
512 Gm resistance. To calculate competitive index, CFUs of *A. tumefaciens* attacker C58
513 strain were divided by the CFUs of target 1D1609 strain at both 0 hr and 16 hr; and the
514 ratio of C58/1D1609 at 16 hr was divided by the ratio of C58/1D1609 at 0 hr to obtain
515 competitive index. One way Analysis of Variance (ANOVA) was used for the analysis of
516 statistical significance followed by the Fishers Least Significant Difference (LSD) test.

517 **Fluorescence microscopy**

518 For propidium iodide and Hoechst staining, *E. coli* cells (BW25113) harbouring Trc200
519 vector or derivatives expressing Tde1 variants were grown overnight and refreshed to a
520 fresh medium as stated for growth inhibition assay. After subculture for 2 hrs, the cells
521 were induced with 1 mM IPTG for one hr and OD_{600} equivalent to 0.3 was collected in 1
522 ml PBS and stained with Hoechst 33342 (H3570) to a final concentration of 12.3 µg/mL
523 and 1 µg/ml Propidium iodide (2208511) and incubated for 2 minutes in dark. Finally, 2
524 µL was spotted on 2.5% agarose pad.

525 For the translocation experiment, the sfGFP fused Tde1 variants were expressed in *A.*
526 *tumefaciens* Δ*tdei* cells (attacker). *E. coli* (target) cells were labelled with mCherry (false
527 colour blue) expressed from pBBRMCS2. *A. tumefaciens* attacker cells were cultured in
528 523 broth overnight, and *E. coli* target cells were separately cultured on LB broth.
529 Overnight cultured attacker and target cells were mixed at 5:1 ratio (OD_{600}= 1.0: 0.2), and

530 10 µL of the mix was cultured on LB-agar plate without IPTG. After 20 hrs of co-culture,
531 the cells were washed with 100 µL PBS and 2 µL of suspension was spotted on the 2.5%
532 agarose pad on a microscopic slide. The merged GFP and mCherry signals was based
533 on a cyan fluorescence.

534 Fluorescence microscopy was performed using Axio Observer 7 (Zeiss, Germany)
535 microscope equipped with an Axiochem 702 digital camera and a Plan-Apochromat
536 100x/1.4 Oil DIC H objective. Exposure times were adjusted to 20 ms for Phase, 50 ms
537 for Hoechst, 150 ms for PI, 200 ms for GFP and 5000 ms for mCherry. Multiple images
538 were taken from different fields and all the experiments were performed at least in
539 triplicate and a representative image is shown. Images were analyzed by using ZEN 2.3
540 (blue edition) software.

541

542 **Domain prediction and analysis**

543 Full-length Tde1 (1-278) was used as a query for conserved domain search on the
544 conserved domains database (CDD) (Lu et al., 2020) of the National Center for
545 Biotechnology Information (NCBI). Prediction of transmembrane domain was done using
546 the PRED-TMR2 (Pasquier et al., 1999). The Tde1 homologues and tape measure proteins
547 (TMPs) for the multiple sequence alignment were obtained by BLAST search of N-Tde1
548 (1-97) against the NCBI non redundant database (nr) with representative sequences
549 selected for multiple sequence alignment. The domain architectures of the Ntox15 domain
550 containing proteins were obtained using the full length Tde1 against Conserved Domain
551 Architectural retrieval tool (CDART) of NCBI. The information of gene clusters encoding
552 Tde1 homologues and TMPs including upstream and downstream three genes was
553 retrieved from their respective genomes. Full-length Tde1 (1-278) was used as a query
554 for structural prediction on a Phyre2 (Kelley et al., 2015). Three-dimensional structure
555 modelling was done using Phyre2 in intensive modelling mode. Crystal structure served
556 as best template for the N-terminus and percentage of confidence for three-dimensional
557 structure modelling are indicated in the legends of corresponding figures. The structural
558 graphics were generated by using ChimeraX 1.1 (Goddard et al., 2018).

559

ACKNOWLEDGEMENT

We would like to thank the Lai lab members for their help and fruitful discussion throughout this study, Yun-Wei Lien for generating the Δ*tdei*Δ*tssK* strain, and Chih-Horng Kuo for discussion and suggestion on BLAST analysis. The authors highly appreciate Jeff Chang, See-Yeun Ting, Lay-Sun Ma, and Chih-Feng Wu for critically reading the manuscript and their valuable comments. We also acknowledge the technical assistance of fluorescence microscope provided by Mei-Jane Fang from Live Cell Imaging Division of Cell Biology Core and Sanger DNA sequencing service provided by Genomic Technology Core, both located at the Institute of Plant and Microbial Biology, Academia Sinica. The authors also thank Ying Wang for illustration of proposed model. The funding was supported by National Science and Technology Council (NSTC) of Taiwan (NSTC 110-2311-B-001-032-MY3) and Academia Sinica Investigator Award (AS-IA-107-L01) to EML. YWC was supported by the postdoctoral fellowship (NSCT 110-2811-B-001-524). The funders had no role in study design, data collection and interpretation, or the decision to submit the work for publication.

AUTHOR CONTRIBUTION

Conceptualization: JA, MY, EML; Investigation: JA, MY, LKS, YWC; Project Funding acquisition and administration: EML; Supervision: EML; Writing of original draft: JA, EML; Writing – methodology, review & editing: JA, MY, LKS, YWC, EML.

REFERENCES

Ahmad, S., Tsang, K.K., Sachar, K., Quentin, D., Tashin, T.M., Bullen, N.P., Raunser, S., McArthur, A.G., Prehna, G., and Whitney, J.C. (2020). Structural basis for effector transmembrane domain recognition by type VI secretion system chaperones. Elife *9*. 10.7554/eLife.62816.

Ali, J., and Lai, E.M. (2022). Distinct TssA proteins converge in coordinating tail biogenesis of the type VI secretion systems. Bioessays, e2200219. 10.1002/bies.202200219.

Atanaskovic, I., Sharp, C., Press, C., Kaminska, R., and Kleanthous, C. (2022). Bacterial Competition Systems Share a Domain Required for Inner Membrane Transport of the Bacteriocin Pyocin G from Pseudomonas aeruginosa. mBio *13*, e0339621. 10.1128/mbio.03396-21.

Baba, T., Ara, T., Hasegawa, M., Takai, Y., Okumura, Y., Baba, M., Datsenko, K.A., Tomita, M., Wanner, B.L., and Mori, H. (2006). Construction of *Escherichia coli* K-12 in-frame, single-gene knockout mutants: the Keio collection. Mol Syst Biol *2*, 2006 0008.

595 Basler, M., Pilhofer, M., Henderson, G.P., Jensen, G.J., and Mekalanos, J.J. (2012). Type VI secretion
596 requires a dynamic contractile phage tail-like structure. Nature *483*, 182-186. nature10846
597 [pii]10.1038/nature10846.

598 Behrens, H.M., Lowe, E.D., Gault, J., Housden, N.G., Kaminska, R., Weber, T.M., Thompson, C.M.A.,
599 Mislin, G.L.A., Schalk, I.J., Walker, D., et al. (2020). Pyocin S5 Import into *Pseudomonas aeruginosa*
600 Reveals a Generic Mode of Bacteriocin Transport. mBio *11*. 10.1128/mBio.03230-19.
601
602 Bondage, D.D., Lin, J.S., Ma, L.S., Kuo, C.H., and Lai, E.M. (2016). VgrG C terminus confers the type VI
603 effector transport specificity and is required for binding with PAAR and adaptor-effector complex. Proc Natl
604 Acad Sci U S A *113*, E3931-3940. 10.1073/pnas.1600428113.
605
606 Casteels, P., Ampe, C., Jacobs, F., and Tempst, P. (1993). Functional and chemical characterization of
607 Hymenoptaecin, an antibacterial polypeptide that is infection-inducible in the honeybee (Apis mellifera). J
608 Biol Chem *268*, 7044-7054.
609
610 Cherrak, Y., Flaugnatti, N., Durand, E., Journet, L., and Cascales, E. (2019). Structure and Activity of the
611 Type VI Secretion System. Microbiol Spectr *7*. 10.1128/microbiolspec.PSIB-0031-2019.
612
613 Cherrak, Y., Rapisarda, C., Pellarin, R., Bouvier, G., Bardiaux, B., Allain, F., Malosse, C., Rey, M., Chamot-
614 Rooke, J., Cascales, E., et al. (2018). Biogenesis and structure of a type VI secretion baseplate. Nat
615 Microbiol *3*, 1404-1416. 10.1038/s41564-018-0260-1.
616
617 Chou, L., Lin, Y.C., Haryono, M., Santos, M.N.M., Cho, S.T., Weisberg, A.J., Wu, C.F., Chang, J.H., Lai,
618 E.M., and Kuo, C.H. (2022). Modular evolution of secretion systems and virulence plasmids in a bacterial
619 species complex. BMC Biol *20*, 16. 10.1186/s12915-021-01221-y.
620
621 Christie, P.J. (2019). The Rich Tapestry of Bacterial Protein Translocation Systems. Protein J *38*, 389-408.
622 10.1007/s10930-019-09862-3.
623
624 Cianfanelli, F.R., Monlezun, L., and Coulthurst, S.J. (2016). Aim, Load, Fire: The Type VI Secretion System,
625 a Bacterial Nanoweapon. Trends Microbiol *24*, 51-62. 10.1016/j.tim.2015.10.005.
626
627 Costa, T.R., Felisberto-Rodrigues, C., Meir, A., Prevost, M.S., Redzej, A., Trokter, M., and Waksman, G.
628 (2015). Secretion systems in Gram-negative bacteria: structural and mechanistic insights. Nat Rev
629 Microbiol *13*, 343-359. 10.1038/nrmicro3456.
630
631 Coulthurst, S. (2019). The Type VI secretion system: a versatile bacterial weapon. Microbiology (Reading)
632 *165*, 503-515. 10.1099/mic.0.000789.
633
634 Cumby, N., Reimer, K., Mengin-Lecreulx, D., Davidson, A.R., and Maxwell, K.L. (2015). The phage tail tape
635 measure protein, an inner membrane protein and a periplasmic chaperone play connected roles in the
636 genome injection process of *E. coli* phage HK97. Mol Microbiol *96*, 437-447. 10.1111/mmi.12918.
637
638 Czolkoss, S., Safronov, X., Rexroth, S., Knoke, L.R., Aktas, M., and Narberhaus, F. (2021). *Agrobacterium*
639 *tumefaciens* Type IV and Type VI Secretion Systems Reside in Detergent-Resistant Membranes. Front
640 Microbiol *12*, 754486. 10.3389/fmicb.2021.754486.
641
642 Durand, E., Nguyen, V.S., Zoued, A., Logger, L., Pehau-Arnaudet, G., Aschtgen, M.S., Spinelli, S.,
643 Desmyter, A., Bardiaux, B., Dujeancourt, A., et al. (2015). Biogenesis and structure of a type VI secretion
644 membrane core complex. Nature *523*, 555-560. 10.1038/nature14667.
645
646 Epand, R.F., Sarig, H., Mor, A., and Epand, R.M. (2009). Cell-wall interactions and the selective
647 bacteriostatic activity of a miniature oligo-acyl-lysyl. Biophys J *97*, 2250-2257. 10.1016/j.bpj.2009.08.006.

Fonte, V., Dostal, V., Roberts, C.M., Gonzales, P., Lacor, P.N., Velasco, P.T., Magrane, J., Dingwell, N., Fan, E.Y., Silverman, M.A., et al. (2011). A glycine zipper motif mediates the formation of toxic beta-amyloid oligomers in vitro and in vivo. Mol Neurodegener *6*, 61. 10.1186/1750-1326-6-61.

Fridman, C.M., Keppel, K., Gerlic, M., Bosis, E., and Salomon, D. (2020). A comparative genomics methodology reveals a widespread family of membrane-disrupting T6SS effectors. Nat Commun *11*, 1085. 10.1038/s41467-020-14951-4.

Garcia-Bayona, L., Guo, M.S., and Laub, M.T. (2017). Contact-dependent killing by *Caulobacter crescentus* via cell surface-associated, glycine zipper proteins. Elife *6*. 10.7554/eLife.24869.

Goddard, T.D., Huang, C.C., Meng, E.C., Pettersen, E.F., Couch, G.S., Morris, J.H., and Ferrin, T.E. (2018). UCSF ChimeraX: Meeting modern challenges in visualization and analysis. Protein Sci *27*, 14-25. 10.1002/pro.3235.

Hachani, A., Wood, T.E., and Filloux, A. (2016). Type VI secretion and anti-host effectors. Curr Opin Microbiol *29*, 81-93. 10.1016/j.mib.2015.11.006.

Hersch, S.J., Lam, L., and Dong, T.G. (2021). Engineered Type Six Secretion Systems Deliver Active Exogenous Effectors and Cre Recombinase. mBio *12*, e0111521. 10.1128/mBio.01115-21.

Ho, B.T., Fu, Y., Dong, T.G., and Mekalanos, J.J. (2017). *Vibrio cholerae* type 6 secretion system effector trafficking in target bacterial cells. Proc Natl Acad Sci U S A *114*, 9427-9432. 10.1073/pnas.1711219114.

Jurenas, D., and Journet, L. (2021). Activity, delivery, and diversity of Type VI secretion effectors. Mol Microbiol *115*, 383-394. 10.1111/mmi.14648.

Kado, C.I., and Heskett, M.G. (1970). Selective media for isolation of *Agrobacterium, Carynebacterium, Erwinia, Pseudomonas,* and *Xanthomonas*. . Phytopathology *60*, 969-976.

Kelley, L.A., Mezulis, S., Yates, C.M., Wass, M.N., and Sternberg, M.J. (2015). The Phyre2 web portal for protein modeling, prediction and analysis. Nat Protoc *10*, 845-858. 10.1038/nprot.2015.053.

Kim, S., Chamberlain, A.K., and Bowie, J.U. (2004). Membrane channel structure of *Helicobacter pylori* vacuolating toxin: role of multiple GXXXG motifs in cylindrical channels. Proc Natl Acad Sci U S A *101*, 5988-5991. 10.1073/pnas.0308694101.

Kim, S., Jeon, T.J., Oberai, A., Yang, D., Schmidt, J.J., and Bowie, J.U. (2005). Transmembrane glycine zippers: physiological and pathological roles in membrane proteins. Proc Natl Acad Sci U S A *102*, 14278-14283. 10.1073/pnas.0501234102.

LaCourse, K.D., Peterson, S.B., Kulasekara, H.D., Radey, M.C., Kim, J., and Mougous, J.D. (2018). Conditional toxicity and synergy drive diversity among antibacterial effectors. Nat Microbiol *3*, 440-446. 10.1038/s41564-018-0113-y.

Lien, Y.W., and Lai, E.M. (2017). Type VI Secretion Effectors: Methodologies and Biology. Front Cell Infect Microbiol *7*, 254. 10.3389/fcimb.2017.00254.

Lin, J.S., Ma, L.S., and Lai, E.M. (2013). Systematic Dissection of the *Agrobacterium* Type VI Secretion System Reveals Machinery and Secreted Components for Subcomplex Formation. PLoS One *8*, e67647. 10.1371/journal.pone.0067647 PONE-D-12-38170 [pii].

Ling, H., Saeidi, N., Rasouliha, B.H., and Chang, M.W. (2010). A predicted S-type pyocin shows a bactericidal activity against clinical *Pseudomonas aeruginosa* isolates through membrane damage. FEBS Lett *584*, 3354-3358. 10.1016/j.febslet.2010.06.021.

Lu, S., Wang, J., Chitsaz, F., Derbyshire, M.K., Geer, R.C., Gonzales, N.R., Gwadz, M., Hurwitz, D.I., Marchler, G.H., Song, J.S., et al. (2020). CDD/SPARCLE: the conserved domain database in 2020. Nucleic Acids Res *48*, D265-D268. 10.1093/nar/gkz991.

Ma, L.S., Hachani, A., Lin, J.S., Filloux, A., and Lai, E.M. (2014). *Agrobacterium tumefaciens* deploys a superfamily of type VI secretion DNase effectors as weapons for interbacterial competition in planta. Cell Host Microbe *16*, 94-104. 10.1016/j.chom.2014.06.002.

Ma, L.S., Lin, J.S., and Lai, E.M. (2009). An IcmF family protein, ImpLM, is an integral inner membrane protein interacting with ImpKL, and its walker a motif is required for type VI secretion system-mediated Hcp secretion in *Agrobacterium tumefaciens*. J Bacteriol *191*, 4316-4329. JB.00029-09 [pii]10.1128/JB.00029-09.

Mariano, G., Trunk, K., Williams, D.J., Monlezun, L., Strahl, H., Pitt, S.J., and Coulthurst, S.J. (2019). A family of Type VI secretion system effector proteins that form ion-selective pores. Nat Commun *10*, 5484. 10.1038/s41467-019-13439-0.

McClain, M.S., Iwamoto, H., Cao, P., Vinion-Dubiel, A.D., Li, Y., Szabo, G., Shao, Z., and Cover, T.L. (2003). Essential role of a GXXXG motif for membrane channel formation by *Helicobacter pylori* vacuolating toxin. J Biol Chem *278*, 12101-12108. 10.1074/jbc.M212595200.

Miyata, S.T., Unterweger, D., Rudko, S.P., and Pukatzki, S. (2013). Dual expression profile of type VI secretion system immunity genes protects pandemic *Vibrio cholerae*. PLoS Pathog *9*, e1003752. 10.1371/journal.ppat.1003752.

Newman, J.R., and Fuqua, C. (1999). Broad-host-range expression vectors that carry the L-arabinose-inducible *Escherichia coli* araBAD promoter and the araC regulator. Gene *227*, 197-203. S0378-1119(98)00601-5 [pii].

Palmer, T., Finney, A.J., Saha, C.K., Atkinson, G.C., and Sargent, F. (2020). A holin/peptidoglycan hydrolase-dependent protein secretion system. Mol Microbiol. 10.1111/mmi.14599.

Pasquier, C., Promponas, V.J., Palaios, G.A., Hamodrakas, J.S., and Hamodrakas, S.J. (1999). A novel method for predicting transmembrane segments in proteins based on a statistical analysis of the SwissProt database: the PRED-TMR algorithm. Protein Eng *12*, 381-385. 10.1093/protein/12.5.381.

Pei, T.T., Li, H., Liang, X., Wang, Z.H., Liu, G., Wu, L.L., Kim, H., Xie, Z., Yu, M., Lin, S., et al. (2020). Intramolecular chaperone-mediated secretion of an Rhs effector toxin by a type VI secretion system. Nat Commun *11*, 1865. 10.1038/s41467-020-15774-z.

Quentin, D., Ahmad, S., Shanthamoorthy, P., Mougous, J.D., Whitney, J.C., and Raunser, S. (2018). Mechanism of loading and translocation of type VI secretion system effector Tse6. Nat Microbiol *3*, 1142-1152. 10.1038/s41564-018-0238-z.

Roessner, C.A., and Ihler, G.M. (1984). Proteinase sensitivity of bacteriophage lambda tail proteins gpJ and pH in complexes with the lambda receptor. J Bacteriol *157*, 165-170. 10.1128/jb.157.1.165-170.1984.

Roessner, C.A., and Ihler, G.M. (1986). Formation of transmembrane channels in liposomes during injection of lambda DNA. J Biol Chem *261*, 386-390.

Ruhe, Z.C., Low, D.A., and Hayes, C.S. (2020). Polymorphic Toxins and Their Immunity Proteins: Diversity, Evolution, and Mechanisms of Delivery. Annu Rev Microbiol *74*, 497-520. 10.1146/annurev-micro-020518-115638.

Russell, A.B., Peterson, S.B., and Mougous, J.D. (2014). Type VI secretion system effectors: poisons with a purpose. Nat Rev Microbiol *12*, 137-148. 10.1038/nrmicro3185.

757 Saint Jean, K.D., Henderson, K.D., Chrom, C.L., Abiuso, L.E., Renn, L.M., and Caputo, G.A. (2018). Effects
758 of Hydrophobic Amino Acid Substitutions on Antimicrobial Peptide Behavior. Probiotics Antimicrob Proteins
759 *10*, 408-419. 10.1007/s12602-017-9345-z.
760
761 Schmidt-Eisenlohr, H., Domke, N., and Baron, C. (1999). TraC of IncN plasmid pKM101 associates with
762 membranes and extracellular high-molecular-weight structures in *Escherichia coli*. J Bacteriol *181*, 5563-
763 5571.
764
765 Vergunst, A.C., Schrammeijer, B., den Dulk-Ras, A., de Vlaam, C.M., Regensburg-Tuink, T.J., and
766 Hooykaas, P.J. (2000). VirB/D4-dependent protein translocation from *Agrobacterium* into plant cells.
767 Science *290*, 979-982. 8951 [pii].
768
769 Vettiger, A., and Basler, M. (2016). Type VI Secretion System Substrates Are Transferred and Reused
770 among Sister Cells. Cell *167*, 99-110 e112. 10.1016/j.cell.2016.08.023.
771
772 Wang, J., Brodmann, M., and Basler, M. (2019). Assembly and Subcellular Localization of Bacterial Type
773 VI Secretion Systems. Annu Rev Microbiol *73*, 621-638. 10.1146/annurev-micro-020518-115420.
774
775 Wettstadt, S., and Filloux, A. (2020). Manipulating the type VI secretion system spike to shuttle passenger
776 proteins. PLoS One *15*, e0228941. 10.1371/journal.pone.0228941.
777
778 Wettstadt, S., Lai, E.M., and Filloux, A. (2020). Solving the Puzzle: Connecting a Heterologous
779 *Agrobacterium tumefaciens* T6SS Effector to a *Pseudomonas aeruginosa* Spike Complex. Front Cell Infect
780 Microbiol *10*, 291. 10.3389/fcimb.2020.00291.
781
782 Wu, C.F., Lien, Y.W., Bondage, D., Lin, J.S., Pilhofer, M., Shih, Y.L., Chang, J.H., and Lai, E.M. (2020).
783 Effector loading onto the VgrG carrier activates type VI secretion system assembly. Embo Rep *21*. ARTN
784 e47961DOI 10.15252/embr.201947961.

785 Wu, C.F., Santos, M.N.M., Cho, S.T., Chang, H.H., Tsai, Y.M., Smith, D.A., Kuo, C.H., Chang, J.H., and
786 Lai, E.M. (2019). Plant-Pathogenic *Agrobacterium tumefaciens* Strains Have Diverse Type VI Effector-
787 Immunity Pairs and Vary in In-Planta Competitiveness. Mol Plant Microbe In *32*, 961-971. 10.1094/Mpmi-
788 01-19-0021-R.
789
790 Wu, C.F., Weisberg, A.J., Davis, E.W., 2nd, Chou, L., Khan, S., Lai, E.M., Kuo, C.H., and Chang, J.H.
791 (2021). Diversification of the Type VI Secretion System in Agrobacteria. mBio *12*, e0192721.
792 10.1128/mBio.01927-21.
793
794 Wu, H.Y., Chung, P.C., Shih, H.W., Wen, S.R., and Lai, E.M. (2008). Secretome Analysis Uncovers an
795 Hcp-Family Protein Secreted via a Type VI Secretion System in *Agrobacterium tumefaciens*. J. Bacteriol
796 *190*, 2841-2850.
797
798 Yu, M., Wang, Y.C., Huang, C.J., Ma, L.S., and Lai, E.M. (2020). *Agrobacterium tumefaciens* Deploys a
799 Versatile Antibacterial Strategy to Increase its Competitiveness. J Bacteriol. 10.1128/JB.00490-20.
800
801 Zhang, D., de Souza, R.F., Anantharaman, V., Iyer, L.M., and Aravind, L. (2012). Polymorphic toxin systems:
802 Comprehensive characterization of trafficking modes, processing, mechanisms of action, immunity and
803 ecology using comparative genomics. Biol Direct *7*, 18. 1745-6150-7-18 [pii]10.1186/1745-6150-7-18.

804 Zoued, A., Durand, E., Brunet, Y.R., Spinelli, S., Douzi, B., Guzzo, M., Flaugnatti, N., Legrand, P., Journet,
805 L., Fronzes, R., et al. (2016). Priming and polymerization of a bacterial contractile tail structure. Nature *531*,
806 59-63. 10.1038/nature17182.

807

808 **FIGURE LEGENDS**

809 **Figure 1. Schematic domain organization, sequence alignment, growth inhibition**
810 **assay of Tde1. (**A) Schematic domain organization of Tde1 protein and its variants. The
811 N-terminal repeated glycine zipper motifs (12-51) overlapping a predicted
812 transmembrane domain (22-42) and Ntox15 DNase domain (99-247) are indicated. Tde1
813 and its variants with truncation or amino acid substitutions were illustrated. (B) Growth
814 inhibition assay of *E. coli* DH10B cells harbouring pTrc200 vector or each of its derivatives
815 expressing Tde1 variants with IPTG induction. (C) Growth inhibition assay of *E. coli*
816 DH10B cells co-expressing the Tde1 variants expressed from pTrc200 plasmid and Tdi1
817 immunity gene expressed from pRL662 plasmid. Growth curve was determined at OD_{600}.
818 Graphs of panels B and C show mean ± SD of three independent experiments. Different
819 letters indicate statistically different groups of strains (p value <0.01). (D) Multiple
820 sequence alignment of N-Tde1 homologues were presented with highly conserved amino
821 acid residues highlighted in yellow. The bacterial species, strain name, and locus number
822 of Tde1 orthologs (*Agrobacterium/Rhizobium*) or tape measure proteins
823 (*Paraburkholderia/Burkholderia*) are indicated on the left and right of aligned sequences.
824 Two conserved glycine residues (G^{39}, G^{43}) subjected for mutagenesis were indicated by
825 the arrows above the sequences.

826

827 **Figure 2. Growth inhibition and membrane permeabilization assays of glycine**
828 **zipper mutants**. (A) Growth inhibition assay of *E. coli* DH10B cells harbouring pTrc200
829 vector or each of its derivatives expressing Tde1 variants with IPTG inducible expression.
830 The growth of *E. coli* was monitored by CFU counting every 1 hr. For membrane
831 permeabilization assays, BW25113 WT or BW25113 (Δ*lacY,* pYTA-*lacZ)* cells harbouring
832 pTrc200 vector or each of its derivatives expressing Tde1 variants were carried out for
833 (B) β-galactosidase activity assay to determine ONPG uptake, (C) propidium iodide
834 permeability with cells treated with Propidium iodide and Hoechst for detection by
835 fluorescence microscope (Scale bar = 5μm). For quantification of cells with PI signals, a
836 total of 6 randomly selected images obtained from two independent experiments were
837 used to quantify the number of PI stained cells / number of Hoechst stained cells as
838 indicated. (D) Bacteriostatic activity assay. *E. coli* DH10B cells harbouring pTrc200 vector

839 or each of its derivatives expressing Tde1 variants were cultured with or without IPTG
840 induction for 1 hr. The IPTG-induced cells were further centrifuged and resuspended in
841 the fresh medium with or without IPTG. Cell density was measured again before
842 continuous growth for additional 1 hr. Graphs of panels A, B, and D show mean ± SD of
843 three independent experiments. Different letters indicate statistically different groups of
844 strains (p value <0.01).

845

846 **Figure 3. The N-terminus of Tde1 is sufficient for interaction with Tap1 and**
847 **secretion. (**A) Co-immunoprecipitation (Co-IP) in *A. tumefaciens. A. tumefaciens* C58
848 Δ*tde1* harbouring pTrc200 vector or its derivatives expressing HA-tagged Tde1 variants.
849 Anti-HA resin was used to coprecipitate the Tde1 variants and Tap1. (B) Secretion assay
850 for HA-tagged Tde1 variants. Western blot for the cellular and extracellular fractions of *A.*
851 *tumefaciens* C58 Δ*tdei* and Δ*tdei1*Δ*tssK* expressing the HA-tagged Tde1 variants. Hcp
852 secretion was detected as a positive control for active T6SS secretion. Representative
853 western blot results of three independent experiments were shown with antibody against
854 HA, Hcp, or EF-Tu serving as a loading and non-secreted protein control. Protein markers
855 are indicated in kDa.

856

857 **Figure 4. Translocation of Tde1 variants fused with sfGFP by *A. tumefaciens-E. coli***
858 **co-culture.** Fluorescence microscopy for Tde1 translocation. *A. tumefaciens* C58 Δ*tdei*
859 expressing Tde1 variants fused with sfGFP (in green) and *E. coli* DH10B carrying
860 mCherry (false coloured in blue) were co-cultured for 20 hrs. A cyan fluorescence with
861 merged blue and green signals represented the translocation of Tde1 variants from *A.*
862 *tumefaciens* to *E. coli* (Scale bar = 5μm). The number of cells with overlayed GFP and
863 mCherry fluorescence was quantified from a total of 6 randomly selected images obtained
864 from three independent experiments (number of cells with cyan fluorescence/ total *E. coli*
865 cells counted).

866

867 **Figure 5. $G^{39}xxxG^{43}$ glycine zipper motif of Tde1 is required for DNase-mediated**
868 **killing of target cells during interbacterial competition. (**A) Interbacterial competition
869 of *A. tumefaciens* C58 Δ*tdei* and Δ*tdei1*Δ*tssK* expressing the Tde1 variants against *E.*
870 *coli* cells was carried out on LB medium and *E. coli* survival rate was quantified by CFU
871 counting. (B) Interbacterial competition between various *A. tumefaciens* C58 strains and
872 *A. tumefaciens* 1D1609 on AK medium and the competition outcome was shown by
873 competitive index. (C) Secretion assay for Tde1 and its variants co-expressed with its
874 immunity protein Tdi1 in *A. tumefaciens* C58 Δ*tdei* and Δ*tdei*Δ*tssK.* (D) *In vivo* plasmid
875 DNA degradation assay. *E. coli* BW25113 carrying pJN105 empty vector or the
876 derivatives expressing different variants of Tde1 were supplemented with 0.5% glucose
877 ("-") or 0.2% L-arabinose ("+") for 3 hrs to either repress or induce Tde1 production. The
878 plasmids were then extracted to observe the DNA degradation and bottom panel
879 showed western blots of specific Tde1 protein bands indicated by arrows. (E) Growth
880 inhibition assay of Tde1 and its variants. *E. coli* BW25113 cells were induced by adding
881 0.2% L-arabinose for Tde1 production. The OD_{600} values were measured every 15
882 minutes. The OD_{600} values of the 4 h post L-arabinose induction were analysed for
883 statistical analysis. Graphs show mean ± SD of three biological repeats. Western blots
884 were detected with specific antibody against Tde1, Hcp, or EF-Tu serving as a loading
885 and non-secreted protein control. Protein markers are indicated in kDa. Data in panel A
886 are mean ± SD of four biological repeats of two independent experiments. Panels B and
887 E show mean ± SD of three independent experiments. Different letters indicate
888 statistically different groups of strains (p value <0.05). Results in panel C and D are
889 representative of three independent experiments.

890

891 **Figure 6. Proposed model of the loading, firing, and translocation of Tde1.** The Tde1
892 translocation is proposed through six steps. Step 1: Tde1 forms a complex with Tdi1 and
893 Tap1 in the attacker cell. Step 2: Tap1-Tde1-Tdi1 complex binds to the VgrG and the
894 Hcp-VgrG-PAAR puncturing device carrying Tde1 effector complex is loaded onto
895 membrane-associated baseplate. Step 3: Hcp tube and TssB/C sheath polymerize on the
896 Tde1-loaded VgrG/baseplate while Tdi1 and Tap1 fall off with unknown mechanisms

897 before or upon firing. Step 4: TssBC sheath contracts and ejects Tde1 into the target cell
898 periplasm or cytoplasm. Step 5: The glycine zipper(s) on the N-terminus of Tde1
899 permeabilize the target cell membrane. Step 6: Intact or truncated Tde1 proteins attack
900 DNA for degradation in the target cell.

901

902

903 **Figure S1. Growth inhibition assays in *A. tumefaciens* and *E. coli*.** (A) Western blot
904 for detection of the expression of HA-tagged Tde1 variants expressed in *E. coli.* *Other
905 HA-tagged truncated bands, related to Figure 1B. (B) Western blot for the detection of
906 Tdi1 from *E. coli* cells co-expressing HA tagged Tde1 variants and strep-tagged Tdi1,
907 related to Figure 1C. (C) Growth inhibition assay of *E. coli* DH10B cells harbouring
908 pTrc200 vector or each of its derivatives expressing Tde1 variants with IPTG inducible
909 expression, monitored by OD_{600}, related to Figure 2A. (D) Growth curve and western blot
910 analyses of *A. tumefaciens* C58 Δ*tde1* carrying pTrc200 or its derivatives expressing HA-
911 tagged Tde1 variants. The growth curve was detected every 2 hrs in 523 medium
912 supplemented with 1 mM IPTG. Graphs show mean ± SD of three independent
913 experiments. Different letters indicate statistically different groups of strains (p value
914 <0.01). The proteins collected at end point (6 hr) were analysed for western blotting with
915 antibody against HA. Representative results of three independent experiments were
916 shown. Protein markers are indicated in kDa. (E) Viability assay for *E. coli* cells derived
917 from the ONPG uptake assay after 1 hr IPTG induction, related to Fig. 2B. (F) The growth
918 curve analysis of *E. coli* cells used for *in vivo* plasmid DNA degradation assay. The
919 turbidity of *E. coli* BW25113 expressing Tde1 and its variants carried out for the *in vivo*
920 plasmid DNA degradation assay were measured. The *E. coli* cells were supplemented
921 with 0.5% glucose (glu) or 0.2% L-arabinose (ara) for the repression or induction of Tde1
922 and its variants. The OD_{600} values were measured by DEN-600 photometer (Biosan,
923 Latvia) every hr.

924

925 **Figure S2. Domain architecture and genetic organizations of Tde homologues.** (A)
926 Domain organization of the Ntox15-containing proteins. Top 10 classes of the Ntox15-

927 containing proteins are shown with the identifiable domains (not to scale). The number of
928 proteins in each class were indicated on the left based on the information on June 29,
929 2022. The *A. tumefaciens* Tde1 belonged to the first class where the N-terminal region
930 lacks an identifiable domain. (B) Genetic organizations of genes encoding Tde1
931 orthologues and Tape Measure Proteins (TMPs) with sequence similarity to N-terminus
932 of Tde1. The proteins encoded from the upstream and downstream of *tde1* and *tmp* genes
933 are shown with their identified domain organizations.
934
935 **Figure S3. Full western blots of Co-IP and secretion assays**
936 (A) Co-IP in *A. tumefaciens. A. tumefaciens* C58 Δ*tde1* harbouring pTrc200 vector or its
937 derivatives expressing HA-tagged Tde1 variants. Anti-HA resin was used to coprecipitate
938 the Tde1 variants and Tap1. (B) Secretion assay for HA-tagged Tde1 variants. Western
939 blot for the cellular and extracellular fractions of *A. tumefaciens* C58 Δ*tdei* and
940 Δ*tdei1*Δ*tssK* expressing the HA-tagged Tde1 variants. Hcp secretion was detected as a
941 positive control for active T6SS secretion. Representative western blot results of three
942 independent experiments were shown with antibody against HA, Hcp, or EF-Tu serving
943 as a loading and non-secreted protein control. Protein markers are indicated in kDa. Box
944 indicates the cropped area shown in Fig. 3.
945
946 **Fig. S4. Fluorescence microscopy for negative controls of translocation assay.**
947 (A) Secretion assay for Tde1 variants fused with sfGFP. Western blot for the cellular and
948 extracellular fractions of *A. tumefaciens* C58 Δ*tdei* and Δ*tdei1*Δ*tssK* expressing the Tde1
949 variants fused with sfGFP were detected by anti-GFP antibody. Representative western
950 blot results of three independent experiments were shown with antibody against GFP,
951 Hcp, or EF-Tu serving as a loading and non secreted protein control. Hcp secretion
952 served as a positive control for active T6SS secretion. Protein markers are indicated in
953 kDa. (B) *A. tumefaciens* C58 Δ*tdei*Δ*tssK* expressing N-Tde1-sfGFP or Tde1(M)-sfGFP (in
954 green) and *E. coli* DH10B carrying mCherry (false coloured in blue) were co-cultured for
955 20 hrs. No cyan fluorescence with merged blue and green signals could be detected when
956 attacker cells are T6SS-inactive, which served as negative controls for the translocation
957 assay (Scale bar = 5μm).

958

959 **Figure S5. Full western blots of secretion assays**

960 Secretion assay for Tde1 and its variants co-expressed with its immunity protein Tdi1 in
961 *A. tumefaciens* C58 Δ*tdei* and Δ*tdei*Δ*tssK***.** Western blots were detected with specific
962 antibody against Tde1, Hcp, or EF-Tu serving as a loading and non-secreted protein
963 control. Protein markers are indicated in kDa. Box indicates the cropped area shown in
964 Fig. 5B, 5E.

965

966 **Figure S6. Structural prediction of the Tde1 N-terminus with similarity to pyocin S5**
967 **and colicins**. (A) Predicted results of N-terminal Tde1 (1-97) as a query. (B) N-terminal
968 Tde1 with structural similarity to pore-forming domain of the pyocin S5, colicines and other
969 membrane perturbing proteins based on Phyre2 prediction. (C) Cartoon model of the
970 Tde1 (residue 10 – 62) by using on the basis of the crystal structure of Pyocin S5 (PDB
971 6THK) with 77.3% of identity. Glycine residues of Tde1 were indicated. (D)
972 Superimposition of N-Tde1 and pore-forming domain of pyocin S5. Tde1 N-terminus is
973 in red and partially pore-forming domain of pyocin S5 is in teal, G^{39} and G^{43} in the putative
974 glycine zipper motif are highlighted in green. All data were analyzed by Phyre2 server.

975

976
977

978

979 **Table S1. List of Strains and plasmids**

Strain/plasmid Name	Relevant Characteristics	Source/Reference	EML No
A. tumefaciens			
C58	Wild type, virulent strain containing nopaline-type Ti plasmid pTiC58	Eugene Nester	EML530
ΔtssL	*tssL* deletion mutant	(Ma et al., 2009)	EML1073
Δtde1	Deletion of *atu4350*		
Δtdei	Deletion of *tde1-tdi1 (atu4350-atu4351)* and *tde2-tdi2 (atu3640-atu3639)* toxin immunity pairs	(Ma *et al.*, 2014)	EML3559
ΔtdeiΔtssK	Deletion of *tssK* in *Δtdei*	This Study	EML5136
E. coli			
DH10B	F- *araDJ39 Δara, leu)7697 ΔlacX74 galU galK rpsL deoR φ80dlacZΔM15 endAI nupG recAI mcrA Δ (mrr hsdRMS mcrBC)*	Invitrogen	EML5396
BW25113	*rrnB Δ lacZ4787 hsdR514 Δ (araBAD)567 DE (rhaBAD)568 rph-1* (ME9062)	NBRP, Japan	EML5398
BW25113 (Δ*lacY*)	*lacY* deletion mutant of the BW25113	NBRP, Japan	
Plasmids			
pTrc200	Sm^R, Sp^R, pVS1 origin *lacIq*, *trc* promoter expression vector	(Schmidt-Eisenlohr et al., 1999)	EML5481
pRL662	Gm^R, non-conjugal transferable broad host range vector derived from pBBR1MCS-2,	(Vergunst et al., 2000)	EML5452
pRL662-Tdi1-Strep	Gm^R, constitutive expression of Tdi1-Strep by *lac* promoter on the pRL662 plasmid	(Ma *et al.*, 2014)	EML3398
pTrc-Tde1(M)-HA	Sp^R, C-terminal HA-tagged Tde1(M) driven by *trc* promoter on pTrc200	This Study	EML5445
pTrc-N-Tde1-HA	Sp^R, N-terminus of Tde1 (1-49) with C-terminal HA tag driven by *trc* promoter on pTrc200	This Study	EML5482
pTrc-N-Tde1^{GLGL}-HA	Sp^R, N-terminus of Tde1 (1-49) with amino acid substitutions (G39L, G43L) and HA tag on C-terminus driven by *trc* promoter on pTrc200	This Study	EML5464
pTrc-Tde1(M)^{GLGL}-HA	Sp^R, C-terminal HA-tagged Tde1(M) with amino acid substitutions (G39L, G43L) driven by *trc* promoter on pTrc200	This study	EML5465
pTrc-C1-Tde1(M)-HA	Sp^R, C-terminus of Tde1(M) (49-278) with C-terminal HA tag driven by *trc* promoter on pTrc200.	This study	EML5479
pTrc-C2-Tde1(WT)-HA	Sp^R, C-terminus of Tde1 (98-278) with C-terminal HA tag driven by *trc* promoter on pTrc200.	This Study	EML5478
pYTA_LacZ	Amp^R, full length *lacZ* gene was cloned on to the YTA vector by TA cloning	This Study	EML1661

pBBRMCS2-mCherry	Km^R, full length mCherry gene was cloned on to pBBRMCS2 plasmid	This Study	EML3022
pTrc200-LacY	Sp^R, *lacY* from BW25113 with C-terminal HA tag driven by *trc* promoter on pTrc200 plasmid.	This Study	EML6350
pTrc-N-Tde1-sfGFP	Sp^R, N-terminus of Tde1 (1-49) fused to the sfGFP on the C-terminal with a GGGS linker driven by *trc* promoter on pTrc200 plasmid	This Study	EML5489
pTrc-N-Tde1^{GLGL}-sfGFP	Sp^R, N-terminus of Tde1 (1-49) with point mutation (G39L, G43L) fused to the sfGFP on the C-terminal with a GGGS linker driven by *trc* promoter on pTrc200 plasmid	This Study	EML5490
pTrc-Tde1(M)-sfGFP	Sp^R, full length of Tde1(M) fused to the sfGFP on the C-terminal with a GGGS linker driven by *trc* promoter on pTrc200 plasmid	This Study	EML5493
pTrc-Tde1(M)^{GLGL}-sfGFP	Sp^R, full length of Tde1(M) with point mutation on (G39L, G43L) fused to the sfGFP on the C-terminal with a GGGS linker driven by *trc* promoter on pTrc200 plasmid	This Study	EML5494
pTrc-C1-Tde1(M)-HA	Sp^R, C-terminus of Tde1 (49-278) fused to the sfGFP on the C-terminal with a GGGS linker driven by *trc* promoter on pTrc200 plasmid	This Study	EML5492
pTrc-C2-Tde1(WT)-HA	Sp^R, C-terminus of Tde1 (98-278) fused to the sfGFP on the C-terminal with a GGGS linker driven by *trc* promoter on pTrc200 plasmid	This Study	EML5491
pTrc200-sfGFP	Sp^R, sfGFP driven by *trc* promoter on pTrc200 plasmid	This Study	EML5495
pTrc-Tde1-Tdi1	Sp^R, expressopm of Tde1-Tdi1 driven by *trc* promoter on pTrc200 plasmid	(Wu et al., 2020)	EML4277
pTrc-Tde1^{GLGL}-Tdi1	SpR, expression of Tde1-Tdi1 driven by trc promoter on pTrc200 plasmid	This Study	EML5513
pTrc-Tde1^{G39L}-Tdi1	SpR, expression Tde1-Tdi1 with point mutation on (G39L) driven by trc promoter on pTrc200 plasmid	This Study	EML6358
pTrc-Tde1^{G43L}-Tdi1	SpR, expression Tde1-Tdi1 with point mutation on (G43L) driven by trc promoter on pTrc200 plasmid	This Study	EML6359
pTrc-Tde1(M)^{GLGL}-Tdi1	SpR, expression Tde1-Tdi1 with point mutation on (G43L) driven by trc promoter on pTrc200 plasmid	This Study	EML6360
pJN105	Gm^R, arabinose-inducible gene expression vector derived from pBBRMCS-1, araC-P_{BAD}	(Newman and Fuqua, 1999)	

pJN105_Tde1	Gm^R, pJN105 expressing C-terminal 6xHis tagged Tde1	This study
pJN105_Tde1^{G39L}	Gm^R, pJN105 expressing C-terminal 6xHis tagged Tde1 with the substitution of G39L	This study
pJN105_Tde1^{G43L}	Gm^R, pJN105 expressing C-terminal 6xHis tagged Tde1 with the substitution of G43L	This study
pJN105_Tde1^{GLGL}	Gm^R, pJN105 expressing C-terminal 6xHis tagged Tde1 with the substitutions of G39L and G43L	This study
pJN105_Tde1(M)	Gm^R, pJN105 expressing C-terminal 6xHis tagged Tde1 with the substitutions of H190A and D193A	This study

980

981

982 **Table S2. List of primers used to make constructs**

Plasmid/Construct made with the primers	Primer names and Sequence (restriction site is indicated underline)
pTrc200_sfGFP	NcoI_sfGFP_F: TGGACCCATGGACCGTAAAGGCGAAGAGCTGTTCA HindIII_sfGFP_R:TCGACAAGCTTTTTGTACAGTTCATCCA TACCATG
pTrc200_Tde1(M)-HA pTrc200_N-Tde1-HA pTrc200_N-Tde1^{GLGL}-HA	NCoI_Tde1_F: AAAAACCATGGACATGAGTGCGACGACAACTGTCG XbaI-Tde1_R: AAAAATCTAGACACCGGGACGTCAGGATTGCC XbaI_N-tde1_R: AAAAATCTAGA A GCT CCC TCA GGC GGA CTA AAG CAA T
pTrc200_C1 Tde1(M)-HA pTrc200_C2-Tde1(M)-HA	NCoI_C2-Tde1_F: AAAAACCATGGACACGCCTAAGCAAGTTGAAGAGTTTAG G NcoI_C1_Tde1_F: AAAAACCATGGACGCGGGTAGAGCGGCTGCCTCCGCAA
pTrc200_N-Tde1^{GLGL}-HA pTrc200_Tde1(M)^{GLGL}-HA pTrc200_Tde1^{GLGL}-Tdi1 pTrc200_Tde1(M)^{GLGL}-Tdi1	G39L_G43L_F: TGGAGGTACAGCGGTTTTAGCATGGATACTTGGGCAAGT CGGCGCTAT G39L_G43L_R: ATAGCGCCGACTTGCCCAAGTATCCATGCTAAAACCGCT GTACCTCCAG
pTrc200_lacY-HA	NcoI_LacY_F: AAAAACCATGGACATGTACTATTTAAAAAACACAAAC XbaI_LacY_R: AAAAATCTAGAAGCGACTTCATTCACCTGACGAC
pTrc200_N-Tde1-sfGFP	N-tde_GGGS_sfGFP_F: TTAGTCCGCCTGAGGGAGCTTCTAGAGGTGGTGGTTCTC GTAAAGGCGAAGAGCTGTT sfGFP_GGGS_Ntde1_R: ACAGCTCTTCGCCTTTACGAGAACCACCACCTCTAGAAG CTCCCTCAGGCGGACTAA
pTrc200_sfGFP	NcoI_sfGFP_F: TGGACCCATGGACCGTAAAGGCGAAGAGCTGTTCA HindIII_sfGFP_R:TCGACAAGCTTTTTGTACAGTTCATCCA TACCATG
pJN105_Tde1	pET-rbs-F1-XbaI: CCCCTCTAGAAATAATTTTGTTTAAC pET-R1-SacI: GGAAGAGCTCCCTTTCGGGCTTTGTTAG

pTrc-Tde1 ^{G39L} -Tdi1	Tde_G39L: FACAGCGGTTCTCGCATGGATAGGTGGGCAATC Tde_G39L_R: GACTTGCCCACCTATCCATGCGAGAACCGCTGT
pTrc-Tde1^{G43L} -Tdi1	Tde_G43L: ACAGCGGTTGGAGCATGGATACTCGGG CAAGTCTde_G43L: GACTTGCCCGAGTATCCATGCTCCAACCGCTGT

983

984

985

986

987

990

Figure 1.

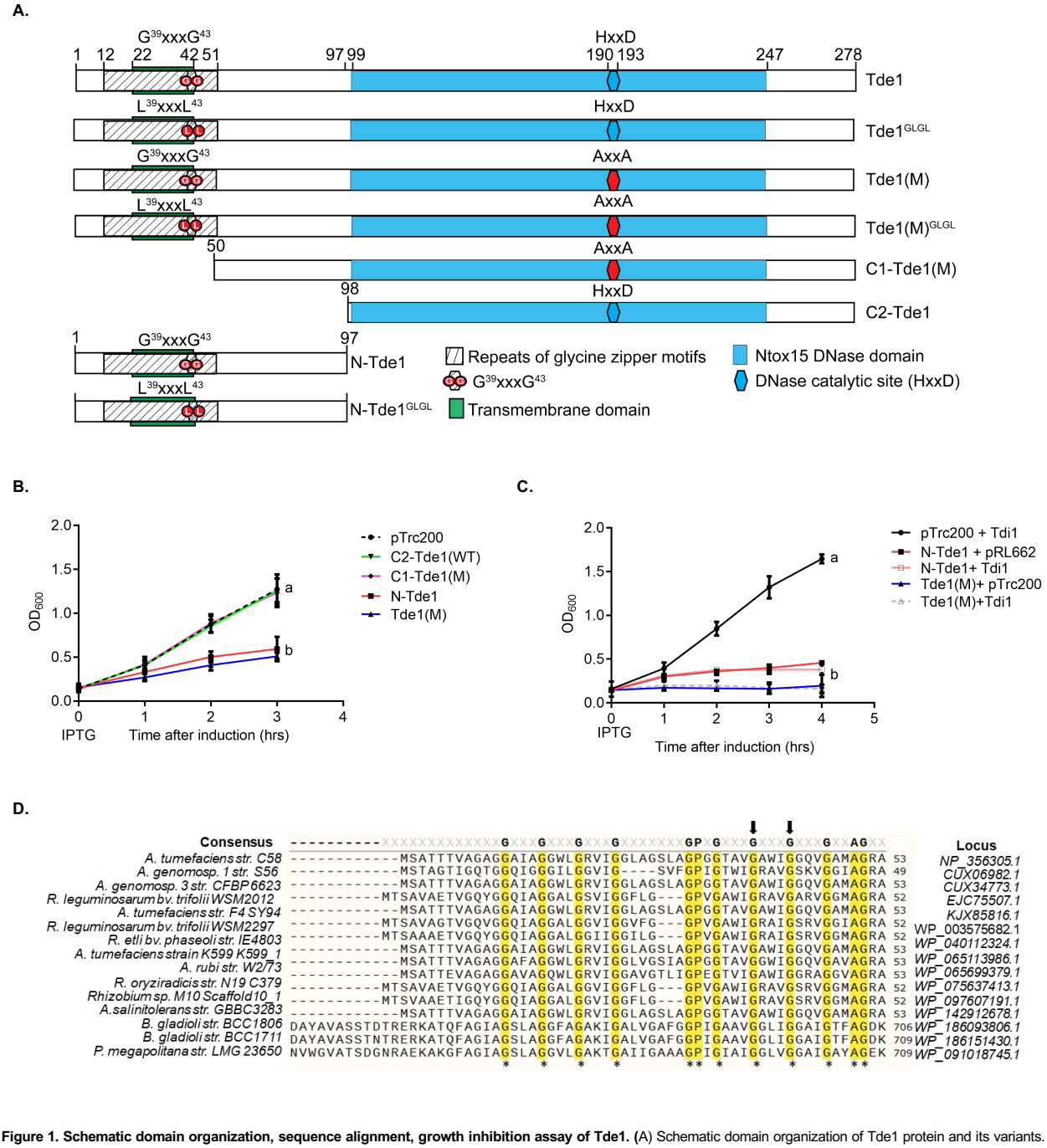

Figure 1. Schematic domain organization, sequence alignment, growth inhibition assay of Tde1. (A) Schematic domain organization of Tde1 protein and its variants. The N-terminal repeated glycine zipper motifs (12-51) overlapping a predicted transmembrane domain (22-42) and Ntox15 DNase domain (99-247) are indicated. Tde1 and its variants with truncation or amino acid substitutions were illustrated. (B) Growth inhibition assay of *E. coli* DH10B cells harbouring pTrc200 vector or each of its derivatives expressing Tde1 variants with IPTG induction. (C) Growth inhibition assay of *E. coli* DH10B cells co-expressing the Tde1 variants expressed from pTrc200 plasmid and Tdi1 immunity gene expressed from pRL662 plasmid. Growth curve was determined at OD_{600}. Graphs of panels B and C show mean ± SD of three independent experiments. Different letters indicate statistically different groups of strains (p value <0.01). (D) Multiple sequence alignment of N-Tde1 homologues were presented with highly conserved amino acid residues highlighted in yellow. The bacterial species, strain name, and locus number of Tde1 orthologs (*Agrobacterium/Rhizobium*) or tape measure proteins (*Paraburkholderia/Burkholderia*) are indicated on the left and right of aligned sequences. Two conserved glycine residues (G^{39}, G^{43}) subjected for mutagenesis were indicated by the arrows above the sequences.

Figure 2

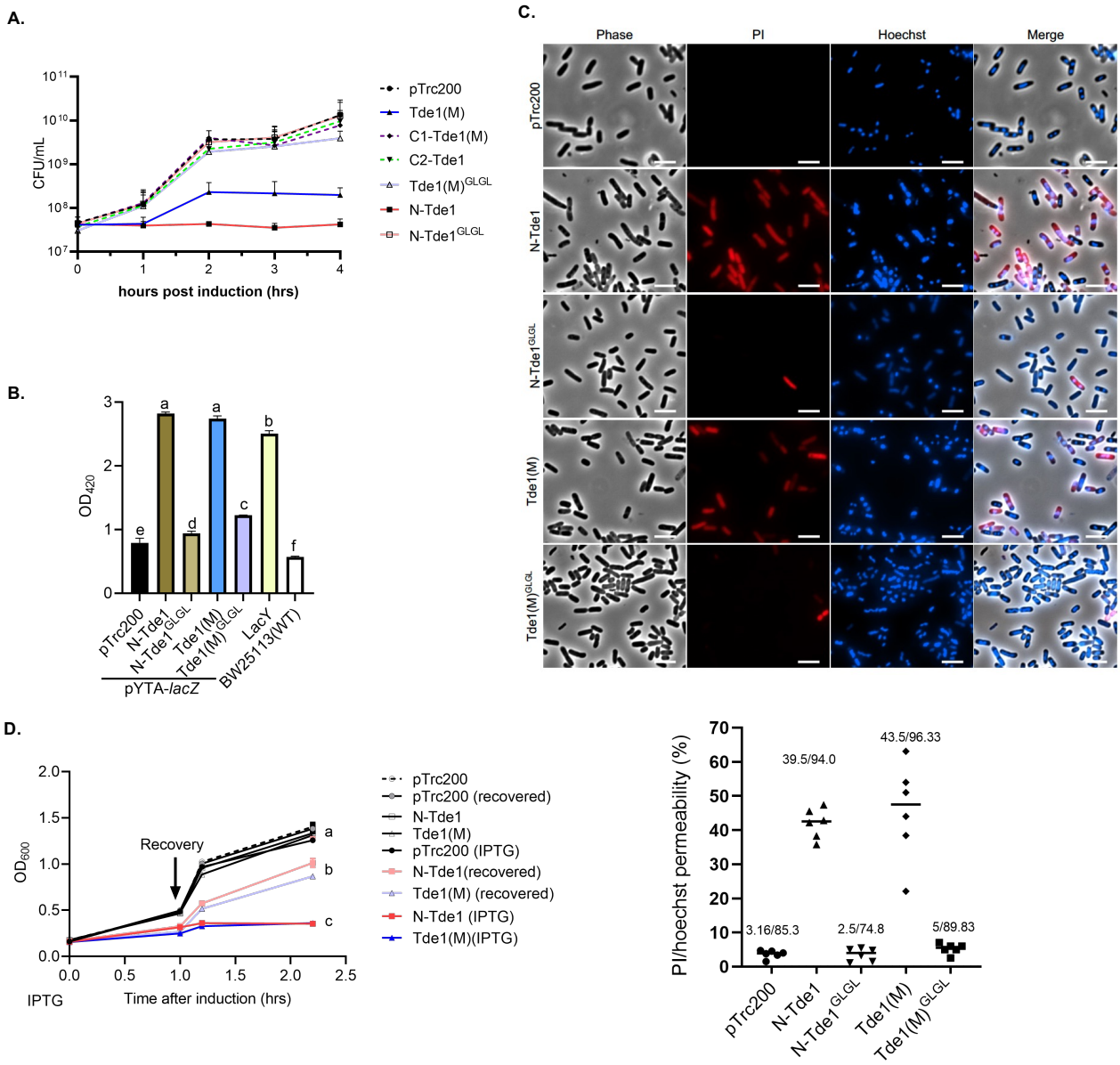

Figure 2. Growth inhibition and membrane permeabilization assays of glycine zipper mutants. (A) Growth inhibition assay of *E. coli* DH10B cells harbouring pTrc200 vector or each of its derivatives expressing Tde1 variants with IPTG inducible expression. The growth of *E. coli* was monitored by CFU counting every 1 hr. For membrane permeabilization assays, BW25113 WT or BW25113 (Δ*lacY,* pYTA-*lacZ)* cells harbouring pTrc200 vector or each of its derivatives expressing Tde1 variants were carried out for (B) β-galactosidase activity assay to determine ONPG uptake, (C) propidium iodide permeability with cells treated with Propidium iodide and Hoechst for detection by fluorescence microscope (Scale bar = 5μm). For quantification of cells with PI signals, a total of 6 randomly selected images obtained from two independent experiments were used to quantify the number of PI stained cells / number of Hoechst stained cells as indicated. (D) Bacteriostatic activity assay. *E. coli* DH10B cells harbouring pTrc200 vector or each of its derivatives expressing Tde1 variants were cultured with or without IPTG induction for 1 hr. The IPTG-induced cells were further centrifuged and resuspended in the fresh medium with or without IPTG. Cell density was measured again before continuous growth for additional 1 hr. Graphs of panels A, B, and D show mean ± SD of three independent experiments. Different letters indicate statistically different groups of strains (p value <0.01).

Figure 3

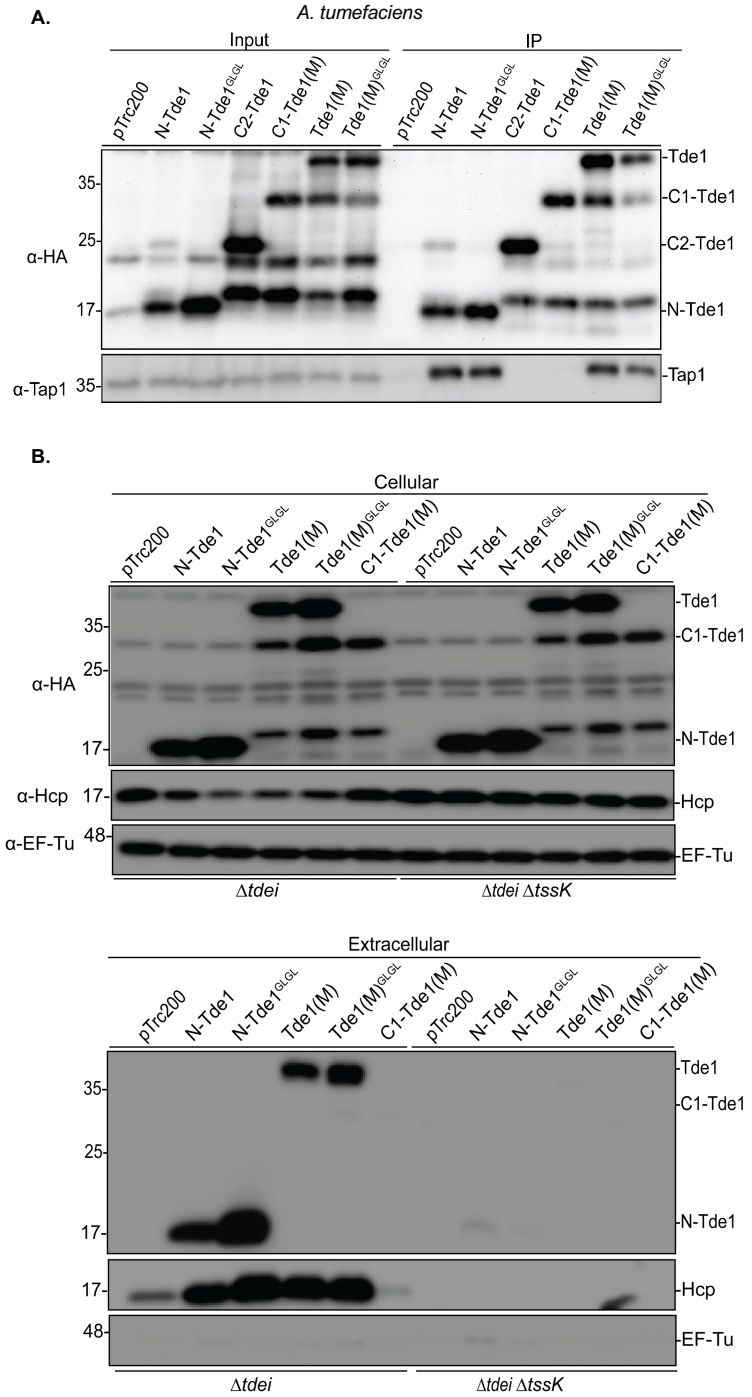

Figure 3. The N-terminus of Tde1 is sufficient for interaction with Tap1 and secretion. (A) Co-immunoprecipitation (Co-IP) in *A. tumefaciens. A. tumefaciens* C58 Δ*tde1* harbouring pTrc200 vector or its derivatives expressing HA-tagged Tde1 variants. Anti-HA resin was used to coprecipitate the Tde1 variants and Tap1. (B) Secretion assay for HA-tagged Tde1 variants. Western blot for the cellular and extracellular fractions of *A. tumefaciens* C58 Δ*tdei* and Δ*tdei1*Δ*tssK* expressing the HA-tagged Tde1 variants. Hcp secretion was detected as a positive control for active T6SS secretion. Representative western blot results of three independent experiments were shown with antibody against HA, Hcp, or EF-Tu serving as a loading and non-secreted protein control. Protein markers are indicated in kDa.

Figure 4

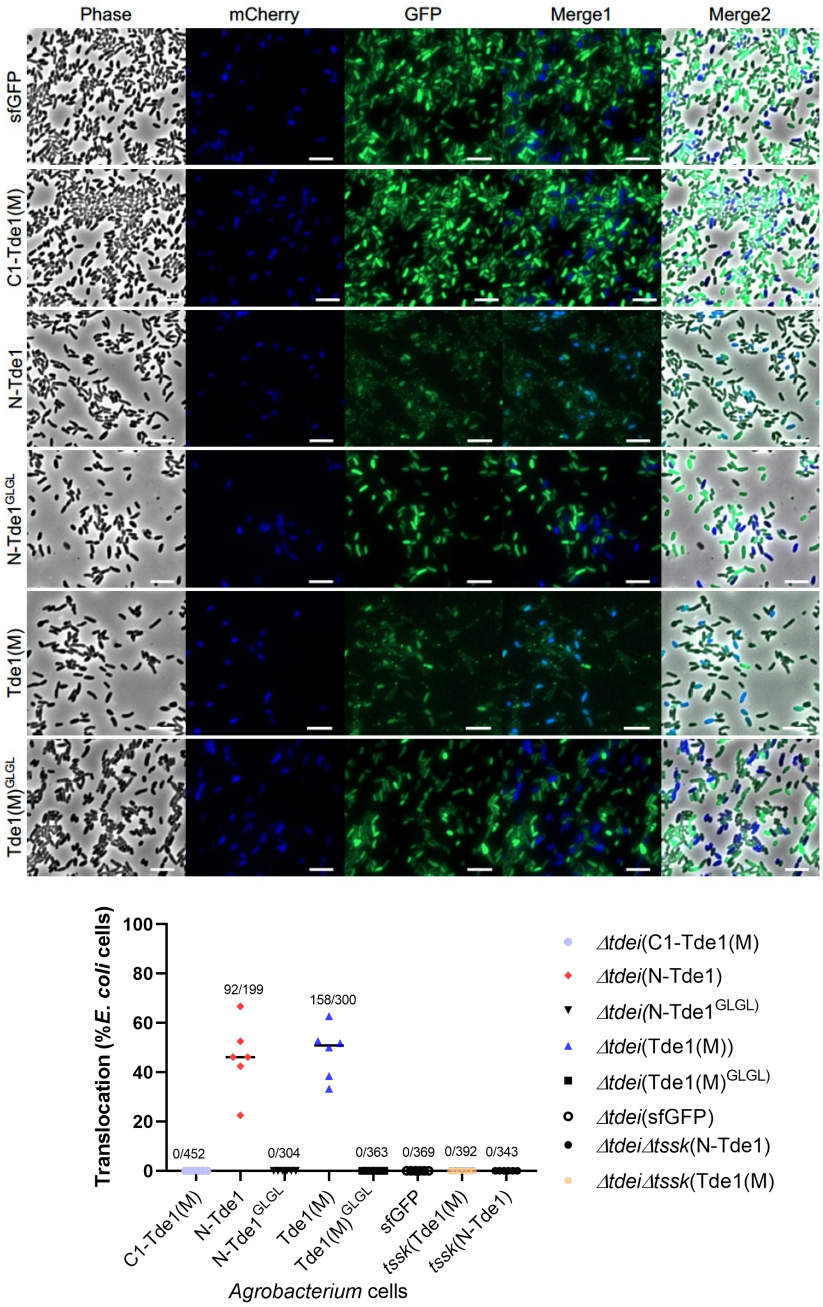

Figure 4. Translocation of Tde1 variants fused with sfGFP by *A. tumefaciens-E. coli* co-culture. Fluorescence microscopy for Tde1 translocation. *A. tumefaciens* C58 Δ*tdei* expressing Tde1 variants fused with sfGFP (in green) and *E. coli* DH10B carrying mCherry (false coloured in blue) were co-cultured for 20 hrs. A cyan fluorescence with merged blue and green signals represented the translocation of Tde1 variants from *A. tumefaciens* to *E. coli* (Scale bar = 5μm). The number of cells with overlayed GFP and mCherry fluorescence was quantified from a total of 6 randomly selected images obtained from three independent experiments (number of cells with cyan fluorescence/ total *E. coli* cells counted).

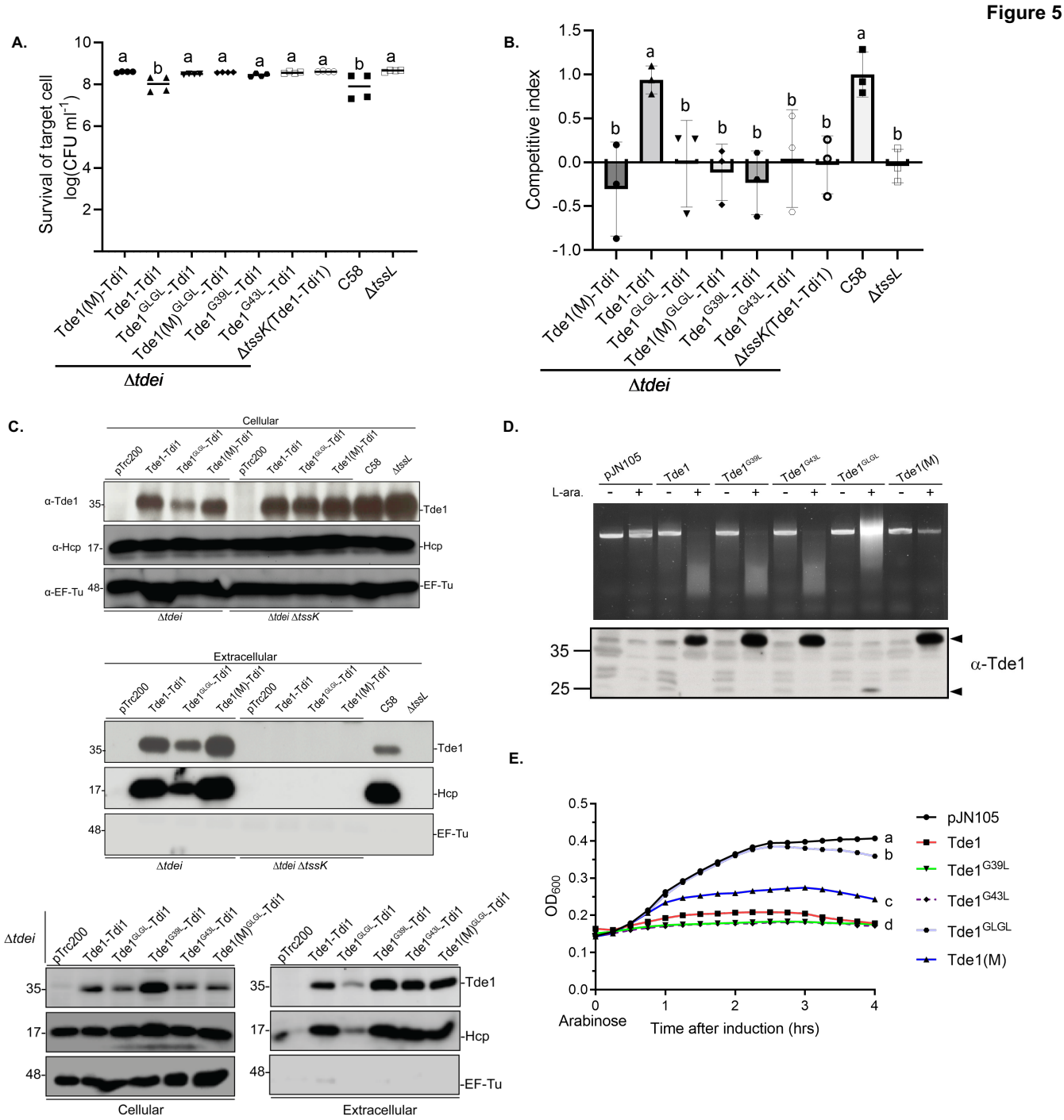

Figure 5. G^{39}xxxG^{43} glycine zipper motif of Tde1 is required for DNase-mediated killing of target cells during interbacterial competition. (A) Interbacterial competition of *A. tumefaciens* C58 Δ*tdei* and Δ*tdei1*Δ*tssK* expressing the Tde1 variants against *E. coli* cells was carried out on LB medium and *E. coli* survival rate was quantified by CFU counting. (B) Interbacterial competition between various *A. tumefaciens* C58 strains and *A. tumefaciens* 1D1609 on AK medium and the competition outcome was shown by competitive index. (C) Secretion assay for Tde1 and its variants co-expressed with its immunity protein Tdi1 in *A. tumefaciens* C58 Δ*tdei* and Δ*tdei*Δ*tssK*. (D) *In vivo* plasmid DNA degradation assay. *E. coli* BW25113 carrying pJN105 empty vector or the derivatives expressing different variants of Tde1 were supplemented with 0.5% glucose ("-") or 0.2% L-arabinose ("+") for 3 hrs to either repress or induce Tde1 production. The plasmids were then extracted to observe the DNA degradation and bottom panel showed western blots of specific Tde1 protein bands indicated by arrows. (E) Growth inhibition assay of Tde1 and its variants. *E. coli* BW25113 cells were induced by adding 0.2% L-arabinose for Tde1 production. The OD_{600} values were measured every 15 minutes. The OD_{600} values of the 4 h post L-arabinose induction were analysed for statistical analysis. Graphs show mean ± SD of three biological repeats. Western blots were detected with specific antibody against Tde1, Hcp, or EF-Tu serving as a loading and non-secreted protein control. Protein markers are indicated in kDa. Data in panel A are mean ± SD of four biological repeats of two independent experiments. Panels B and E show mean ± SD of three independent experiments. Different letters indicate statistically different groups of strains (p value <0.05). Results in panel C and D are representative of three independent experiments.

Figure 6

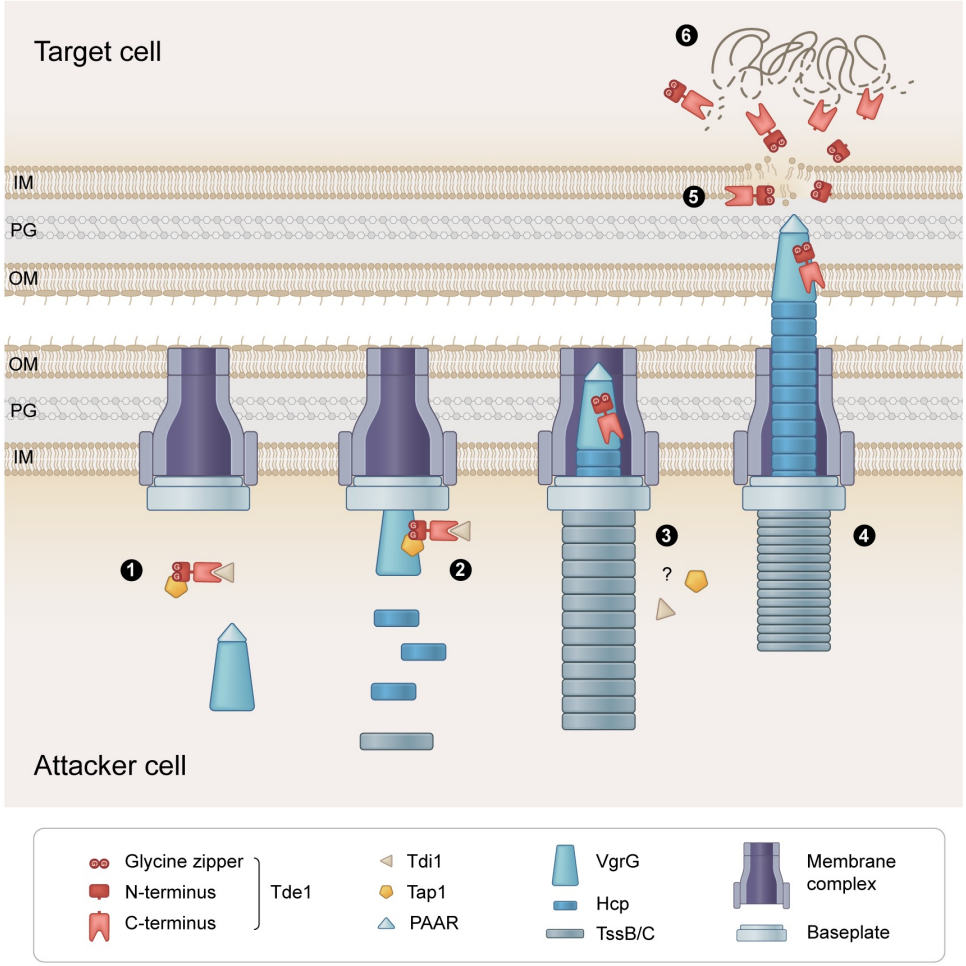

Figure 6. Proposed model of the loading, firing, and translocation of Tde1. The Tde1 translocation is proposed through six steps. Step 1: Tde1 forms a complex with Tdi1 and Tap1 in the attacker cell. Step 2: Tap1-Tde1-Tdi1 complex binds to the VgrG and the Hcp-VgrG-PAAR puncturing device carrying Tde1 effector complex is loaded onto membrane-associated baseplate. Step 3: Hcp tube and TssB/C sheath polymerize on the Tde1-loaded VgrG/baseplate while Tdi1 and Tap1 fall off with unknown mechanisms before or upon firing. Step 4: TssBC sheath contracts and ejects Tde1 into the target cell periplasm or cytoplasm. Step 5: The glycine zipper(s) on the N-terminus of Tde1 permeabilize the target cell membrane. Step 6: Intact or truncated Tde1 proteins attack DNA for degradation in the target cell.

Figure S1

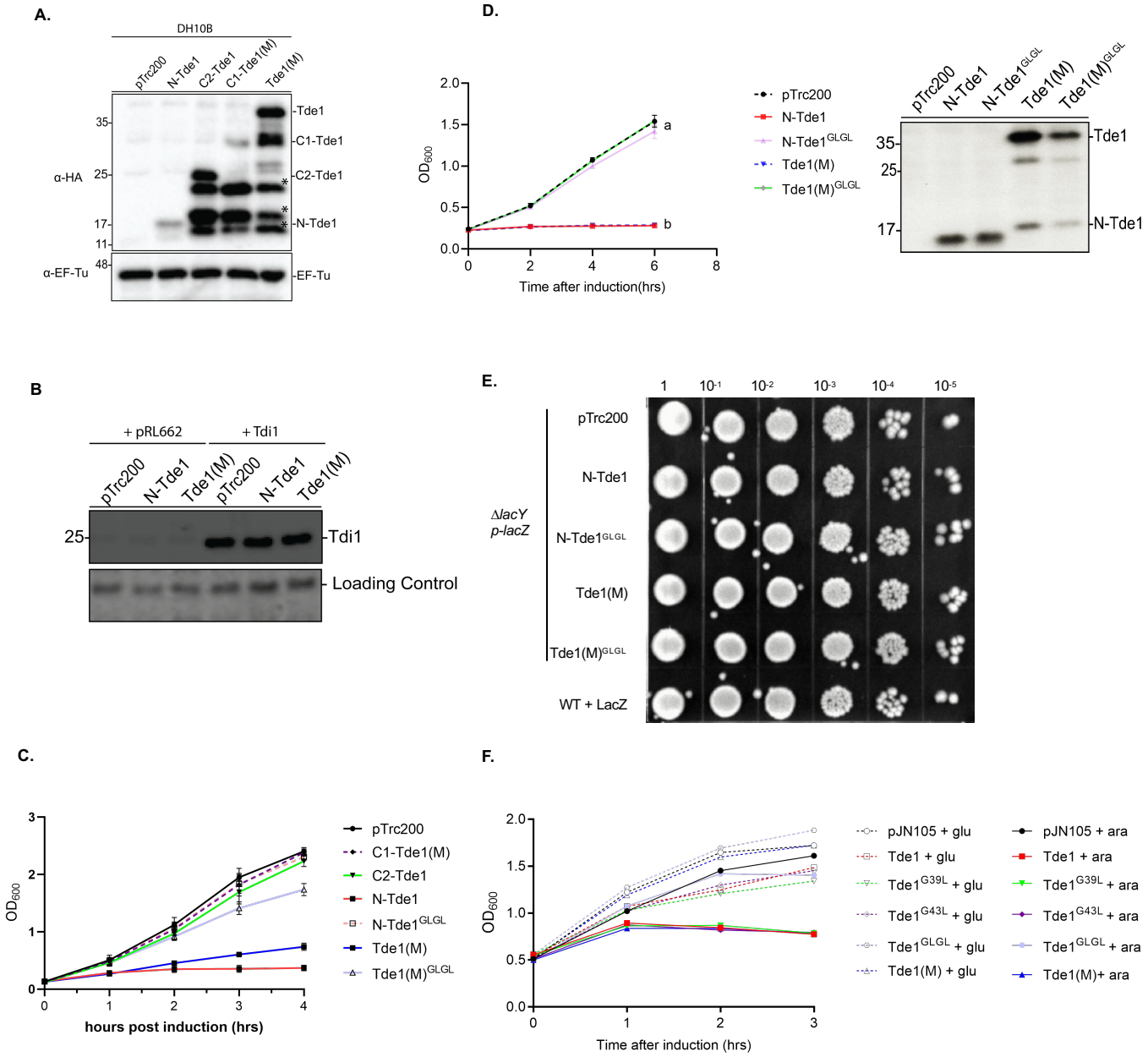

Figure S1. Growth inhibition assays in *A. tumefaciens* and *E. coli*. (A) Western blot for detection of the expression of HA-tagged Tde1 variants expressed in *E. coli.* *Other HA-tagged truncated bands, related to Figure 1B. (B) Western blot for the detection of Tdi1 from *E. coli* cells co-expressing HA tagged Tde1 variants and strep-tagged Tdi1, related to Figure 1C. (C) Growth inhibition assay of *E. coli* DH10B cells harbouring pTrc200 vector or each of its derivatives expressing Tde1 variants with IPTG inducible expression, monitored by OD_{600}, related to Figure 2A. (D) Growth curve and western blot analyses of *A. tumefaciens* C58 Δ*tde1* carrying pTrc200 or its derivatives expressing HA-tagged Tde1 variants. The growth curve was detected every 2 hrs in 523 medium supplemented with 1 mM IPTG. Graphs show mean ± SD of three independent experiments. Different letters indicate statistically different groups of strains (p value <0.01). The proteins collected at end point (6 hr) were analysed for western blotting with antibody against HA. Representative results of three independent experiments were shown. Protein markers are indicated in kDa. (E) Viability assay for *E. coli* cells derived from the ONPG uptake assay after 1 hr IPTG induction, related to Fig. 2B. (F) The growth curve analysis of *E. coli* cells used for *in vivo* plasmid DNA degradation assay. The turbidity of *E. coli* BW25113 expressing Tde1 and its variants carried out for the *in vivo* plasmid DNA degradation assay were measured. The *E. coli* cells were supplemented with 0.5% glucose (glu) or 0.2% L-arabinose (ara) for the repression or induction of Tde1 and its variants. The OD_{600} values were measured by DEN-600 photometer (Biosan, Latvia) every hr.

Figure S2

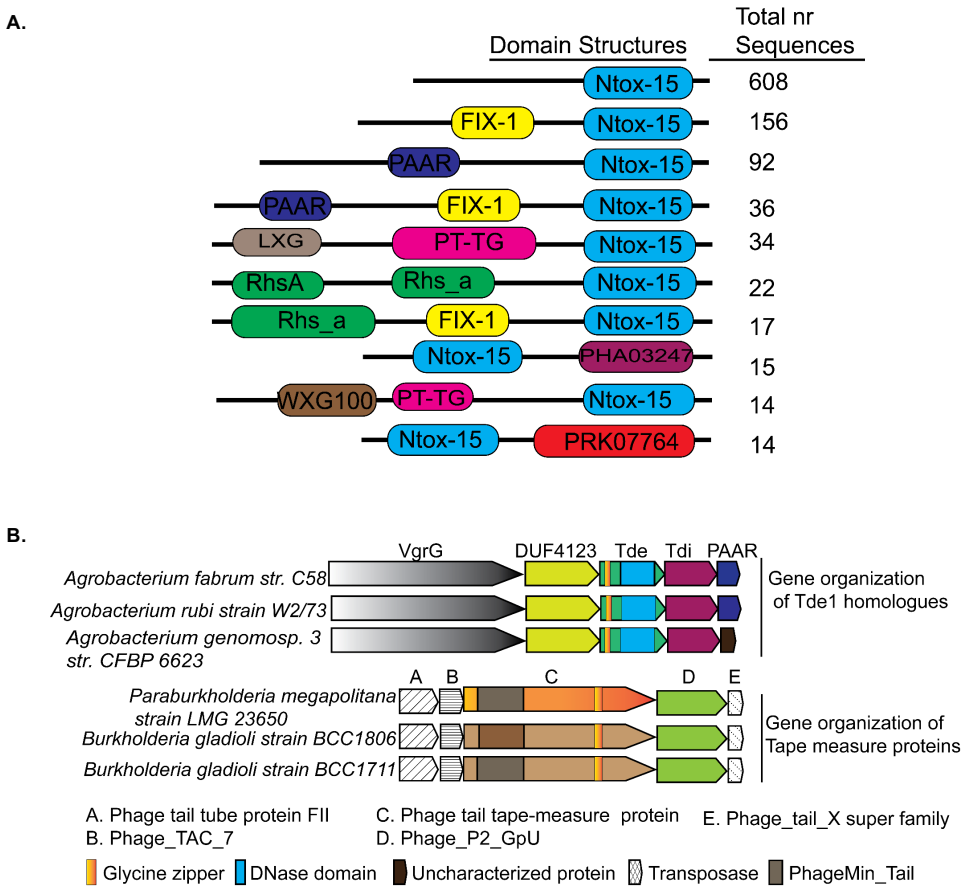

Figure S2. Domain architecture and genetic organizations of Tde homologues. (A) Domain organization of the Ntox15-containing proteins. Top 10 classes of the Ntox15-containing proteins are shown with the identifiable domains (not to scale). The number of proteins in each class were indicated on the left based on the information on June 29, 2022. The *A. tumefaciens* Tde1 belonged to the first class where the N-terminal region lacks an identifiable domain. (B) Genetic organizations of genes encoding Tde1 orthologues and Tape Measure Proteins (TMPs) with sequence similarity to N-terminus of Tde1. The proteins encoded from the upstream and downstream of *tde1* and *tmp* genes are shown with their identified domain organizations.

Figure S3

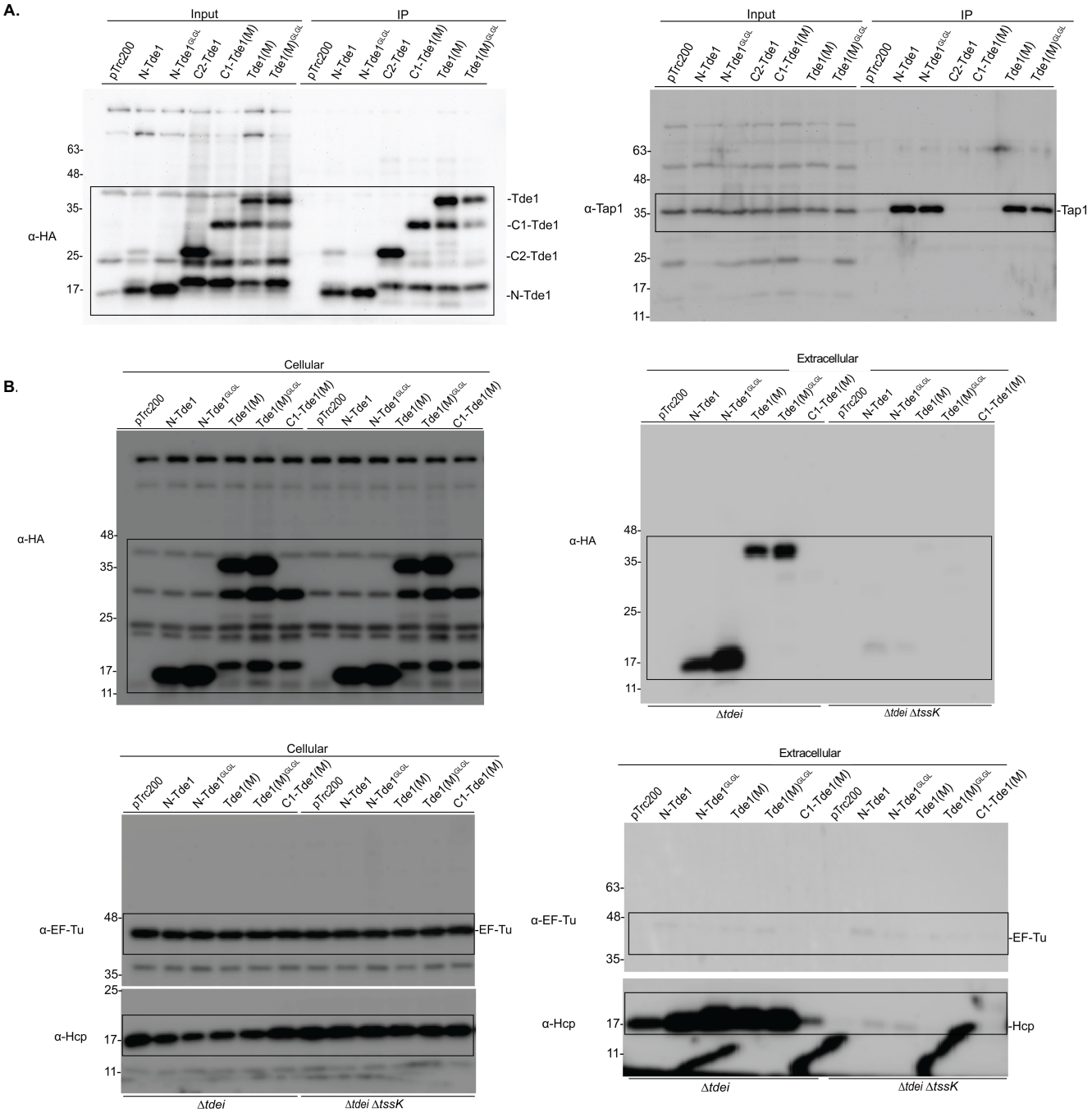

Figure S3. Full western blots of Co-IP and secretion assays

(A) Co-immunoprecipitation (Co-IP) in *A. tumefaciens*. *A. tumefaciens* C58 Δ*tde1* harbouring pTrc200 vector or its derivatives expressing HA-tagged Tde1 variants. Anti-HA resin was used to coprecipitate the Tde1 variants and Tap1. (B) Secretion assay for HA-tagged Tde1 variants. Western blot for the cellular and extracellular fractions of *A. tumefaciens* C58 Δ*tdei* and Δ*tdei1*Δ*tssK* expressing the HA-tagged Tde1 variants. Hcp secretion was detected as a positive control for active T6SS secretion. Representative western blot results of three independent experiments were shown with antibody against HA, Hcp, or EF-Tu serving as a loading and non-secreted protein control. Protein markers are indicated in kDa. Box indicates the cropped area shown in Fig. 3.

Figure S4

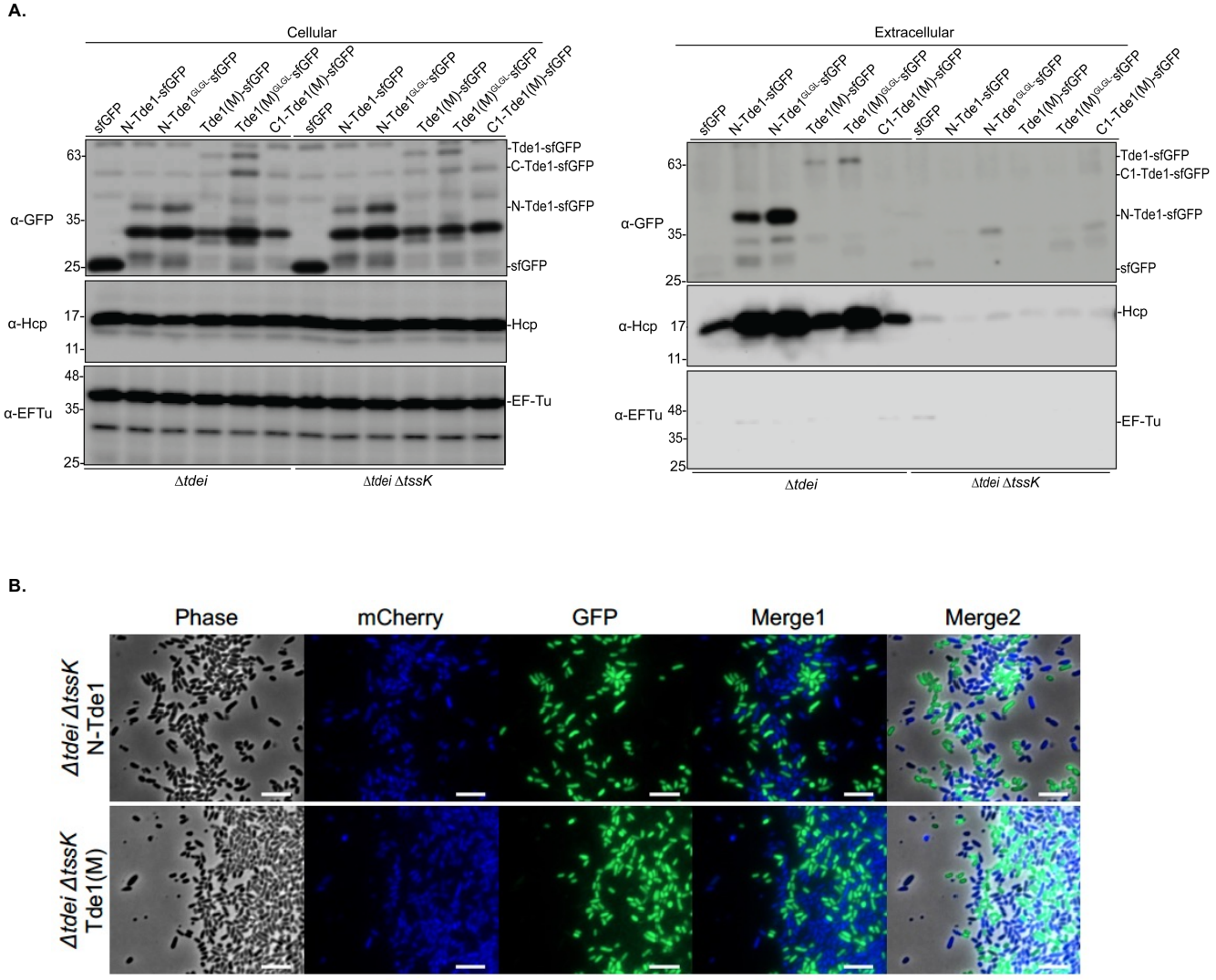

Fig. S4. Fluorescence microscopy for negative controls of translocation assay. (A) Secretion assay for Tde1 variants fused with sfGFP. Western blot for the cellular and extracellular fractions of *A. tumefaciens* C58 Δ*tdei* and Δ*tdei1*Δ*tssK* expressing the Tde1 variants fused with sfGFP were detected by anti-GFP antibody. Representative western blot results of three independent experiments were shown with antibody against GFP, Hcp, or EF-Tu serving as a loading and non secreted protein control. Hcp secretion served as a positive control for active T6SS secretion. Protein markers are indicated in kDa. (B) *A. tumefaciens* C58 Δ*tdei*Δ*tssK* expressing N-Tde1-sfGFP or Tde1(M)-sfGFP (in green) and *E. coli* DH10B carrying mCherry (false coloured in blue) were co-cultured for 20 hrs. No cyan fluorescence with merged blue and green signals could be detected when attacker cells are T6SS-inactive, which served as negative controls for the translocation assay (Scale bar = 5μm).

Figure S5

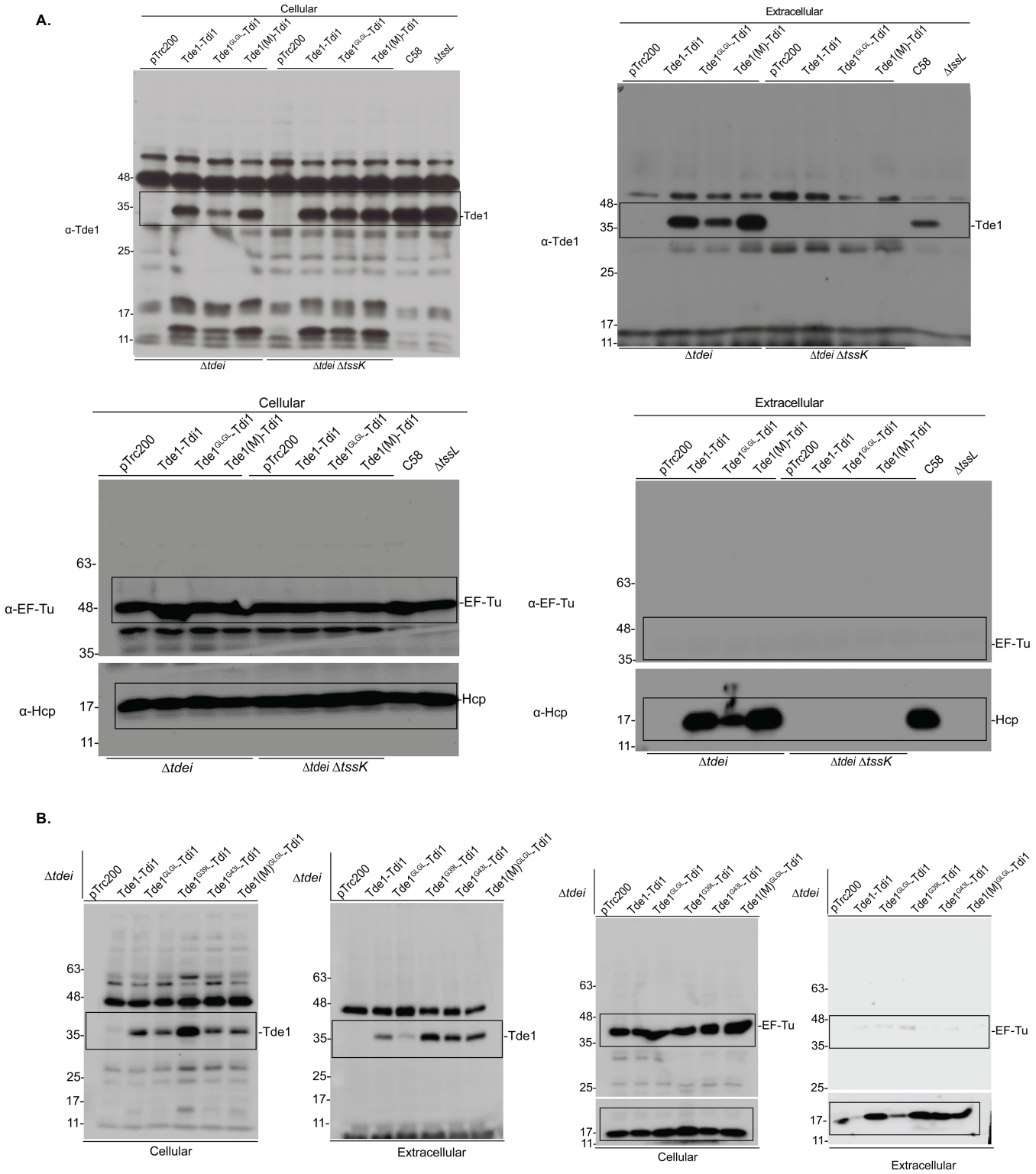

Figure S5. Full western blots of secretion assays

Secretion assay for Tde1 and its variants co-expressed with its immunity protein Tdi1 in *A. tumefaciens* C58 Δ*tdei* and Δ*tdei*Δ*tssK*. Western blots were detected with specific antibody against Tde1, Hcp, or EF-Tu serving as a loading and non-secreted protein control. Protein markers are indicated in kDa. Box indicates the cropped area shown in Fig. 5B, 5E.

Figure S6

A.

Positions on Tde1	Alignment Coverage	3D Model	Confidence	% i.d.	Template Information
10-62	Alignment		77.3	26	**PDB header:**antimicrobial protein **Chain:** A: **PDB Molecule:**pyocin s5; **PDBTitle:** structural mechanism of pyocin s5 import into pseudomonas aeruginosa **PDB Entry:** PDBe RCSB PDBj ✓ View investigator results
14-58	Alignment		69.5	18	**PDB header:**transmembrane protein **Chain:** A: **PDB Molecule:**colicin ia; **PDBTitle:** colicin ia **PDB Entry:** PDBe RCSB PDBj Run Investigator
7-62	Alignment		33.0	25	**Fold:** Toxins' membrane translocation domains **Superfamily:** Colicin **Family:** Colicin **PDB entry:** PDBe RCSB PDBj Run Investigator
19-51	Alignment		27.6	50	**PDB header:**viral protein/inhibitor **Chain:** C: **PDB Molecule:**envelope glycoprotein b; **PDBTitle:** hcmv prefusion gb in complex with fusion inhibitor way-174865 **PDB Entry:** PDBe RCSB PDBj Run Investigator
4-62	Alignment		27.4	27	**PDB header:**immune system **Chain:** X: **PDB Molecule:**colicin s4; **PDBTitle:** structure and function of colicin s4, a colicin with a duplicated2 receptor binding domain **PDB Entry:** PDBe RCSB PDBj Run Investigator

B.

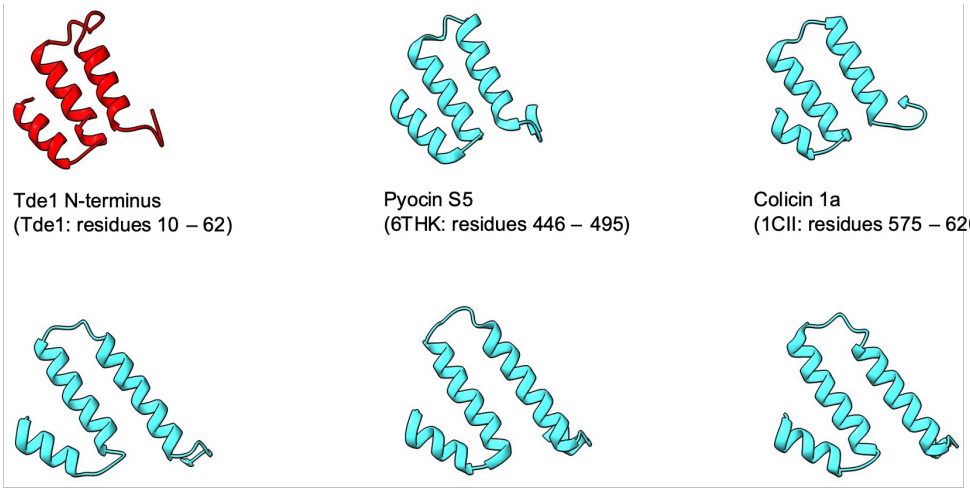

C.

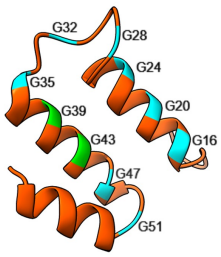

D.

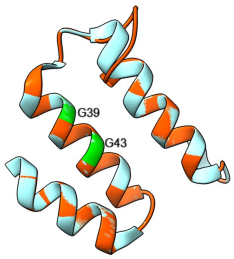

Figure S6. Structural prediction of the Tde1 N-terminus with similarity to pyocin S5 and colicins. (A) Predicted results of N-terminal Tde1 (1-97) as a query. (B) N-terminal Tde1 with structural similarity to pore-forming domain of the pyocin S5, colicines and other membrane perturbing proteins based on Phyre2 prediction. (C) Cartoon model of the Tde1 (residue 10 – 62) by using on the basis of the crystal structure of Pyocin S5 (PDB 6THK) with 77.3% of identity. Glycine residues of Tde1 were indicated. (D) Superimposition of N-Tde1 and pore-forming domain of pyocin S5. Tde1 N-terminus is in red and partially pore-forming domain of pyocin S5 is in teal, G^{39} and G^{43} in the putative glycine zipper motif are highlighted in green. All data were analyzed by Phyre2 server.